d^0 Metal Olefin Complexes. Synthesis, Structures, and Dynamic Properties of $(C_5R_5)_2Zr(OCMe_2CH_2CH_2CH{=}CH_2)^+$ Complexes: Models for the Elusive $(C_5R_5)_2Zr(R)(Olefin)^+$ Intermediates in Metallocene-Based Olefin Polymerization Catalysis

Jean-François Carpentier, Zhe Wu, Chul Woo Lee, Staffan Strömberg, Joseph N. Christopher, and Richard F. Jordan*

Contribution from the Department of Chemistry, The University of Chicago, 5735 South Ellis Avenue, Chicago, Illinois 60637

Received March 20, 2000

Abstract: To model the Zr−olefin interaction in the as-yet unobserved $(C_5R_5)_2Zr(R)(olefin)^+$ intermediates in $(C_5R_5)_2Zr(R)^+$-catalyzed olefin polymerization, the coordination of the tethered vinyl group in $(C_5R_5)_2Zr(OCMe_2(CH_2)_nCH{=}CH_2)^+$ species has been investigated. The reaction of $(C_5H_5)_2Zr(OCMe_2CH_2CH_2CH{=}CH_2)(Me)$ with $B(C_6F_5)_3$ or $[Ph_3C][B(C_6F_5)_4]$ yields the chelated olefin complex $(C_5H_5)_2Zr(OCMe_2CH_2CH_2CH{=}CH_2)^+$ as the $MeB(C_6F_5)_3^-$ (**12a**) or $B(C_6F_5)_4^-$ (**12b**) salts. In contrast, the reaction of $(C_5H_5)_2Zr(OCMe_2CH_2CH{=}CH_2)(Me)$ with $B(C_6F_5)_3$ in CD_2Cl_2 yields the $MeB(C_6F_5)_3^-$ adduct $(C_5H_5)_2Zr^{(+)}(OCMe_2CH_2CH{=}CH_2)(\mu\text{-}Me)B^{(-)}(C_6F_5)_3$. The reaction of $(C_5H_5)_2Zr(OCMe_2CH_2CH_2CH_2CH{=}CH_2)(Me)$ with $B(C_6F_5)_3$ yields a 1.2/1 mixture (at −90 °C) of the chelated olefin complex $(C_5H_5)_2Zr(OCMe_2CH_2CH_2CH_2CH{=}CH_2)^+$ and the $MeB(C_6F_5)_3^-$ adduct $(C_5H_5)_2Zr^{(+)}(OCMe_2CH_2CH_2CH{=}CH_2)(\mu\text{-}Me)B^{(-)}(C_6F_5)_3'$. The reaction of *rac*-(EBI)-$Zr(OCMe_2CH_2CH_2CH{=}CH_2)(Me)$ (EBI = ethylene-1,2-bis(1-indenyl)) with $B(C_6F_5)_3$ or $[Ph_3C][B(C_6F_5)_4]$ yields the chelated olefin complex *rac*-(EBI)$Zr(OCMe_2CH_2CH_2CH{=}CH_2)^+$ as the $MeB(C_6F_5)_3^-$ (**20a**) or $B(C_6F_5)_4^-$ (**20b**) salts, each as a 1/1 mixture of diastereomers which differ in the relative configuration of the *rac*-(EBI)-Zr unit and the internal carbon of the coordinated olefin. X-ray diffraction analyses of **12a** and the *S,S,R*/*R,R,S* isomer of **20a**, and NMR data for **12a**,**b** and **20a**,**b** establish that the Zr−olefin bonding in these species is unsymmetrical and consists of a weak $Zr-C_{term}$ interaction and minimal $Zr-C_{int}$ interaction (**12a**, $Zr-C_{term}$ = 2.68(2), $Zr-C_{int}$ = 2.89(2) Å; **20a**, $Zr-C_{term}$ = 2.634(5), $Zr-C_{int}$ = 2.819(4) Å). X-ray ($d_{C=C}$), IR ($\nu_{C=C}$), and NMR (^1H, ^{13}C) data show that the Zr−olefin interaction does not significantly perturb the structure of the coordinated olefin but does polarize the C=C bond such that positive charge buildup occurs at C_{int}. Similar unsymmetrical bonding and polarization effects may contribute to the high insertion reactivity of $(C_5R_5)_2Zr(R)(\alpha\text{-olefin})^+$ species. Dynamic NMR studies show that **12a**,**b** and **20a**,**b** undergo olefin face exchange in solution on the NMR time scale. The free energy barrier for face exchange of **20a** ($\Delta G^{\ddagger}_{FE}$ = 15.4(4) kcal/mol at 43 °C) is significantly greater than that for **12a** ($\Delta G^{\ddagger}_{FE}$ = 10.7(5) kcal/mol at −55 °C). Possible origins of this difference are discussed. The face exchange of **20a** is dissociative, with minimal involvement of anion, solvent, or σ-complex intermediates.

Introduction

Olefin complexes of d^0 transition metals play a key role in several important processes that are catalyzed by high-oxidation-state early metal complexes, including olefin polymerization and ring-opening metathesis polymerization (ROMP).[1,2] In the case of insertion polymerization of olefins, d^0 metal alkyl−olefin and hydride−olefin species, i.e., $L_nM(R)(olefin)$ and $L_nM(H)(olefin)$, are key intermediates in chain growth (insertion) and chain transfer (β-H and β-alkyl elimination). The characterization of species of this type, or models thereof, is of interest for understanding the coordination and activation of olefins by d^0 metal centers, catalyst structure/reactivity/selectivity relationships, stereocontrol in α-olefin polymerization, the competition between olefins, Lewis bases and counterions for binding to active catalyst species, and other issues of relevance to olefin polymerization. However, d^0 metal olefin complexes are extremely rare and little is known about their structures, bonding or dynamic properties. Metal−olefin bonding in d^0 complexes is anticipated to be weak due to the absence of conventional $d-\pi^*$ back-bonding.[3] Furthermore, in many cases d^0 metal olefin complexes can undergo facile reactions, such as insertion and ligand exchange.[4]

Two types of simple (i.e., nonchelated) d^0 metal olefin adducts have been observed and characterized by NMR spectroscopy (Chart 1). The cationic W^{VI} cycloheptene cyclopentylidene

(1) (a) Boor, J., Jr. *Ziegler−Natta Catalysts and Polymerizations*; Academic: New York, 1979. (b) Van der Ven, S. *Polypropylene and Other Polyolefins*; Elsevier: Amsterdam, 1990. (c) Tait, P. J. In *Comprehensive Polymer Science*; Allen, G., Berington, J. C., Eds.; Pergamon: Oxford, UK, 1989; Vol. 4, pp 1−25.

(2) (a) Ivin, K. J.; Mol, J. C. *Olefin Metathesis and Metathesis Polymerization*; Academic: London, 1997. (b) Schrock, R. R. *Acc. Chem. Res.* **1990**, *23*, 158. (c) Novak, B. M.; Risse, W.; Grubbs, R. H. *The Development of Well-Defined Catalysts for Ring-Opening Olefin Metathesis Polymerizations (ROMP)*; Polymer Synthesis Oxidation Processes 102; Springer-Verlag: Berlin, 1992. (d) Feldman, J. R.; Schrock, R. R. *Prog. Inorg. Chem.* **1991**, *39*, 1. (e) Gilliom, L. R.; Grubbs, R. H. *J. Am. Chem. Soc.* **1986**, *108*, 733.

10.1021/ja000989p CCC: $19.00
Published on Web 07/22/2000

Chart 1

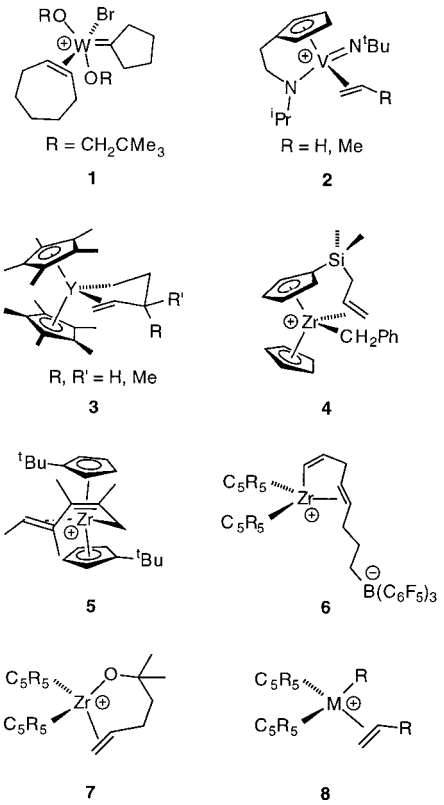

species **1** is formed reversibly by the reaction of cycloheptene and W(cyclopentylidene)$(OR)_2$Br$(BrGaBr_3)$ at low temperature, and initiates cycloheptene ROMP above ca. −25 °C.[5] NMR data indicate that **1** has a trigonal bipyramidal structure with a parallel alignment of the C═C and W═C bonds, and suggest that the structure of the olefin is not significantly perturbed by coordination to W^{VI}. Several analogues of **1** were also detected by low-temperature NMR. The V^V ethylene and propylene complexes **2** have also been detected by NMR.[6] These species form reversibly upon exposure of the bromobenzene adduct $\{\eta^5$:η^1-$C_5H_4CH_2CH_2N^iPr\}V(N^tBu)(C_6D_5Br)^+$ to the olefin. Computational results for the model compound $\{\eta^5$:η^1-$C_5H_4CH_2$-$CH_2NH\}V(NH)$(ethylene)$^+$ predict that the C═C bond is aligned parallel to the V═NH bond and that the ethylene is coordinated in an unsymmetrical fashion. It is possible that weak π(W═C)−π*(olefin) and π(V═N)−π*(olefin) back-bonding stabilizes **1** and **2**.

Several chelated olefin complexes of d^0 metals have also been reported (Chart 1). The Y^{III} alkyl−olefin adducts **3** are formed by reaction of $\{(C_5Me_5)_2YH\}_2$ with the appropriate diene and are stable below ca. −50 °C.[7] Low-temperature NMR studies of **3** show that olefin face-exchange is rapid on the NMR time scale even at −100 °C, suggesting that the Y-olefin interaction is quite weak. The cationic Zr species **4** is generated by benzyl abstraction from Cp(η^5-$C_5H_4SiMe_2CH_2CH$═CH_2)Zr$(CH_2Ph)_2$ (Cp = C_5H_5) using $B(C_6F_5)_3$ or CPh_3^+ and was characterized by NMR.[8] The vinyl ^{1}H and ^{13}C NMR resonances of **4** are significantly shifted from those of the neutral precursor, which confirms that the pendant olefin rather than the benzyl phenyl group is coordinated to Zr. The cationic σ,π,π-pentadienyl complex **5** is formed by the reaction of $(C_5H_4{}^tBu)_2$Zr(Me)$(NMe_2$-Ph)$^+$ and 2-butyne.[9] The localized pentadienyl bonding and weak Zr−olefin interactions were confirmed by X-ray crystallography. Several related cationic vinyl−olefin species, e.g., **6**, have also been described.[10] In many of these chelated olefin complexes, the structure of the M−olefin unit and the strength of the M−olefin bond may be strongly influenced by structural constraints imposed by the tether.[11−13]

The objective of the present work is to develop a general approach for the synthesis of d^0 metal olefin complexes that can be utilized to study the structures, bonding, reactivity, and dynamic properties of a variety of systems relevant to olefin polymerization catalysis. The strategy described here is based on the use of the linked alkoxide−olefin ligand −$OCMe_2CH_2$-CH_2CH═CH_2, for which monodentate (**A**) and chelated (**B**) binding modes are illustrated in eq 1. This ligand was chosen for several reasons. (i) It was envisioned that cationic d^0 metal alkoxide species **A** could be generated from the parent alcohol and appropriate metal alkyls L_nMR_2 by standard alkane elimination/alkyl abstraction reaction sequences as illustrated generically in eq 1, and that the chelate effect would favor formation of

(3) Weak d^0 metal−olefin binding has been detected by several techniques. (a) Charge-transfer complexes between $TiCl_4$ and olefins: Krauss, H. L.; Nickl, J. *Z. Naturforsch.* **1965**, *B20*, 630. (b) Gas chromatographic evidence for weak binding of ethylene to $M(CH_2Ph)_4$/squalene/diatomite and $M(CH_2SiMe_3)_4$/diatomite (M = Zr, Hf): Ballard, D. G. H.; Burnham, D. R.; Twose, D. L. *J. Catal.* **1976**, *44*, 116. (c) Paramagnetic NMR evidence for ethylene binding to $(C_5Me_5)_2$Eu (d^{0}f^7): Nolan, S. P.; Marks, T. J. *J. Am. Chem. Soc.* **1989**, *111*, 8538.

(4) The d^6 species (C_5Me_5)Co$\{P(OMe)_3\}(C_2H_4)(Et)^+$ and d^8 (diimine)-M(R)(olefin)$^+$ (M = Pd, Pt) species have been characterized. (a) Brookhart, M.; Volpe, A. F.; Lincoln, D. M.; Horvath, I. T.; Millar, J. M. *J. Am. Chem. Soc.* **1990**, *112*, 5634. (b) Rix, F. C.; Brookhart, M. *J. Am. Chem. Soc.* **1995**, *117*, 5634. (c) Johnson, L. K.; Mecking, S.; Brookhart, M. *J. Am. Chem. Soc.* **1996**, *118*, 267. (d) Fusto, M.; Giordano, F.; Orabona, I.; Ruffo, F.; Panunzi, A. *Organometallics* **1997**, *16*, 5981.

(5) Kress, J.; Osborn, J. A. *Angew. Chem., Int. Ed. Engl.* **1992**, *31*, 1585.

(6) Witte, P. T.; Meetsma, A.; Hessen, B. *J. Am. Chem. Soc.* **1997**, *119*, 10561.

(7) (a) Casey, C. P.; Hallenbeck, S. L.; Pollock, D. W.; Landis, C. R. *J. Am. Chem. Soc.* **1995**, *117*, 9770. (b) Casey, C. P.; Hallenbeck. S. L.; Wright, J. M.; Landis, C. R. *J. Am. Chem. Soc.* **1997**, *119*, 9681. (c) Casey, C. P.; Fagan, M. A.; Hallenbeck, S. L. *Organometallics* **1998**, *17*, 287. (d) Analogous zwitterionic Zr(IV) complexes, $Cp^*_2Zr^{(+)}\{\eta^1,\eta^2$-$CH_2CH(CH_2$-$B^{(-)}(C_6F_5)_3)CH_2CH$═$CH_2\}$, have been reported recently. Casey, C. P.; Carpenetti, D. W.; Sakuri, H. *J. Am. Chem. Soc.* **1999**, *121*, 9483.

(8) Galakhov, M. V.; Heinz, G.; Royo, P. *J. Chem. Soc., Chem. Commun.* **1998**, 17.

(9) Horton, A. D.; Orpen, A. G. *Organometallics* **1992**, *11*, 8.

(10) (a) Karl, J.; Dahlmann, M.; Erker G.; Bergander, K. *J. Am. Chem. Soc.* **1998**, *120*, 5643. (b) Ahlers, W.; Erker, G.; Frölich, R. *Eur. J. Inorg. Chem.* **1998**, 889. (c) Karl, J.; Erker, G. *J. Mol. Catal. A: Chem.* **1998**, *128*, 858. (d) Temme, B.; Karl, J.; Erker, G. *Chem. Eur. J.* **1996**, *2*, 919. (e) Ruwwe, J.; Erker, G.; Frölich, R. *Angew. Chem., Int. Ed. Engl.* **1996**, *35*, 80. (f) Erker, G.; Noe, R.; Krüger, C.; Werner, R. *Organometallics* **1992**, *11*, 4174.

(11) For d^0 metal complexes containing *uncoordinated* tethered olefins see: (a) Okuda, J.; Du Plooy, K. E.; Toscano, P. J. *J. Organomet. Chem.* **1995**, *495*, 195. (b) Clark, R. J. H.; Coles, M. A. *J. Chem. Soc., Dalton Trans.* **1974**, 1462. (c) Clark, R. J. H.; Stockwell, J. A.; Wilkins, J. D. *J. Chem. Soc., Dalton Trans.* **1976**, 120. (d) Okuda, J.; Zimmerman, K. H. *J. Organomet. Chem.* **1988**, *344*, C1. (e) Dõtz, K. H.; Rott, J. *J. Organomet. Chem.* **1988**, *338*, C11. (f) Baldwin, D. A.; Clark, R. J. H. *J. Chem. Soc. A* **1971**, 1725. (g) Butakoff, K. A.; Lemenovskii, P.; Mountford, P.; Kuz'mina, L. G.; Churakov, A. V. *Polyhedron* **1996**, *15*, 489.

(12) For chelated Al alkyl olefin species see: (a) Hata, G. *J. Chem. Soc., Chem. Commun.* **1968**, 7. (b) Dolzine, T. W.; Oliver, J. P. *J. Am. Chem. Soc.* **1974**, *96*, 1737.

(13) For d^0 metal arene complexes see: (a) Bochmann, M.; Karger, G.; Jaggar, A. J. *J. Chem. Soc., Chem. Commun.* **1990**, 1038. (b) Bochmann, M.; Jaggar, A. J.; Nicholls, J. C. *Angew. Chem., Int. Ed. Engl.* **1990**, *29*, 780. (c) Solari, E.; Floriani, C.; Chiesi-Villa, A.; Guastini, C. *J. Chem. Soc., Chem. Commun.* **1989**, 1747. (d) Cotton, F. A.; Schowtzer, W. *J. Am. Chem. Soc.* **1986**, *108*, 4657. (e) Schaverien, C. J. *Organometallics* **1992**, *11*, 3476. (f) Gillis, D. J.; Tudoret, M.; Baird, M. C. *J. Am. Chem. Soc.* **1993**, *115*, 2543. (g) Pellecchia, C.; Grassi, A.; Immirzi, A. *J. Am. Chem. Soc.* **1993**, *115*, 1160. (h) Pellecchia, C.; Immirzi, A.; Grassi, A.; Zambelli, A. *Organometallics* **1993**, *12*, 4473. (i) Pellecchia, C.; Grassi, A.; Zambelli, A. *J. Mol. Catal.* **1993**, *82*, 57. (j) Lancaster, S. J.; Robinson, O. B.; Bochmann, M.; Coles, S. J.; Hursthouse, M. B. *Organometallics* **1995**, *14*, 2456. (k) Horton, A. D.; Fryns, J. H. G. *Angew. Chem., Int. Ed. Engl.* **1991**, *30*, 1152.

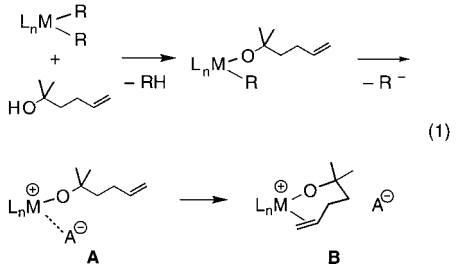

olefin adducts **B** if suitable weakly coordinating anions were used.[14] (ii) Incorporation of alkyl substituents at the alkoxide carbon should disfavor alkoxide abstraction or formation of dinuclear dicationic μ-alkoxide species, and may promote ring closure to **B**.[15] (iii) As a major objective of this study is to probe d^0 metal−olefin bonding, it is important that the linking group in the alkoxide−olefin ligand be sufficiently flexible that it does not strongly perturb this bonding interaction. The utilization of the M−O−CR_2− unit in **A** and **B** is important in this regard. As pointed out by Parkin et al., there is essentially no correlation between Zr−O bond distances and Zr−O−C bond angles in an extensive series of $(C_5R_5)_2Zr(OR')X$ aryloxide and alkoxide compounds.[16] This observation suggests that the Zr−O−C bond angle can be varied over a wide range with minimal effect on the Zr−O bond energy; i.e., the potential energy surface for Zr−O−C bond angle deformation is rather flat. Similar results may be expected for other d^0 metal species.[17] The alkyl tether between the alkoxide and olefin groups also contributes to the flexibility of the chelate ring in **B**.

In this paper we describe the synthesis, structures, and reactivity of $(C_5R_5)_2Zr(OCMe_2CH_2CH_2CH{=}CH_2)^+$ species (**7**, Chart 1). The chelated d^0 olefin complexes **7** are designed to model the as-yet unobserved $(C_5R_5)_2Zr(R)(\alpha\text{-olefin})^+$ cations (**8**) that are key intermediates in metallocene-based olefin polymerization.[18] The structural results reported here provide insights into the nature of Zr^{IV}−olefin bonding that have important implications for the structures and reactivity of **8** and related d^0 metal olefin adducts. Additionally, we report on dynamic NMR studies which provide information concerning the barriers and mechanism of olefin face exchange processes (dissociation/association). Some aspects of this work have been communicated.[19] In the following paper in this series,[20] we will describe analogous studies of $\{\eta^5{:}\eta^1\text{-}C_5R_4SiMe_2N^tBu\}Ti(OCMe_2CH_2CH_2CH{=}CH_2)^+$ species, which are models for the presumed $\{\eta^5{:}\eta^1\text{-}C_5R_4TiSiMe_2N^tBu\}Ti(R)(olefin)^+$ intermediates in the recently developed "constrained geometry" catalyst systems.[21]

Results

$(C_5H_5)_2Zr\{OCMe_2(CH_2)_nCH{=}CH_2\}(Me)$ (n = 1−3) Complexes. The reaction of Cp_2ZrMe_2 with the olefinic alcohols $HOCMe_2(CH_2)_nCH{=}CH_2$ (n = 1−3) yields alkoxide complexes **9**−**11** (Scheme 1). The NMR parameters for the vinyl groups of **9**−**11** are unchanged from the free olefin values, indicating that the vinyl groups are not coordinated. In particular, the vinyl ^{13}C NMR resonances for **9** (δ C_{int} 113.9, C_{term} 140.4) are not shifted from the corresponding resonances for the parent alcohol (δ 113.9, 140.0).

Synthesis and Structure of $Cp_2Zr(OCMe_2CH_2CH_2CH{=}CH_2)^+$. The reaction of **9** with $B(C_6F_5)_3$ in CH_2Cl_2 yields $[Cp_2Zr(OCMe_2CH_2CH_2CH{=}CH_2)][MeB(C_6F_5)_3]$ (**12a**), which can be isolated (94%) as an analytically pure, yellow crystalline solid by recrystallization from CH_2Cl_2/pentane.[22] NMR data establish that the vinyl group in **12a** coordinates to Zr in CD_2Cl_2 solution. The terminal vinyl ^{13}C resonance shifts upfield (δ C_{term} 94.3) and the internal vinyl ^{13}C resonance shifts downfield (δ C_{int} 158.8) by ca. 20 ppm from the corresponding resonances of the free olefin and **9**. Similarly, the vinyl ^1H resonances are substantially shifted from those of the free olefin and **9**; in particular, the H_{int} resonance shifts from δ 5.86 for **9** to δ 7.50 in **12a**.[23] The low-temperature (−80 °C) ^1H NMR spectrum of **12a** contains two singlets for the diastereotopic Cp groups and two singlets for the diastereotopic $ZrOCMe_2$− groups, as expected for the chelated structure. These pairs of resonances each collapse to a singlet at higher temperatures due to rapid olefin face exchange as discussed in detail below. The NMR parameters for the $MeB(C_6F_5)_3^-$ anion of **12a** (B*Me*, 23 °C, CD_2Cl_2: ^1H NMR, δ 0.5 br; ^{13}C NMR, δ 10.1 br) are identical to those for $[NBu_3CH_2Ph][MeB(C_6F_5)_3]$, which establishes that the counterion in **12a** is not coordinated to Zr.

The IR spectra of **12a** under a variety of conditions contain a $\nu_{C=C}$ band at 1641 cm^{-1} which is virtually unshifted from those in the free olefin and THF adduct $[Cp_2Zr(OCMe_2CH_2CH_2CH{=}CH_2)(THF)][MeB(C_6F_5)_3]$ (**13**, Scheme 1, vide infra). Additionally, the J_{C-H} coupling constants for the vinyl carbons of **12a** (C_{int}, 151 Hz; C_{term}, 154 Hz) are nearly identical to the corresponding values for the free olefin (151, 156 Hz) and **13** (152, 156 Hz). These observations indicate that the structure of the vinyl group (i.e., C=C bond distance, R−C−H and H−C−H angles) is not significantly perturbed by coordination to Zr.[24]

The solid-state molecular structure of **12a** was determined by X-ray diffraction as described in detail in the preliminary

(14) Recent reviews concerning weakly coordinating anions: (a) Strauss, S. H. *Chem. Rev.* **1993**, *93*, 927. (b) Reed, C. A. *Acc. Chem. Res.* **1998**, *31*, 133. (c) Lupinetti, A. J.; Strauss, S. H. *Chemtracts−Inorg. Chem.* **1972**, *11*, 565. See also: (d) Jia, L.; Yang, X.; Stern, C. L.; Marks, T. J. *Organometallics* **1997**, *16*, 842. (e) Chen, Y.-X.; Metz, M. V.; Li, L.; Stern, C. L.; Marks, T. J. *J. Am. Chem. Soc.* **1998**, *120*, 6287. (f) Deck, P. A.; Beswick, C. L.; Marks, T. J. *J. Am. Chem. Soc.* **1998**, *120*, 1772.

(15) For examples of d^0 $(L_nM)_2(\mu\text{-}X)_2^{2+}$ species (X = OH, OR, halide) see: (a) Martin, A.; Uhrhammer, R.; Gardner, T. G.; Jordan, R. F.; Rogers, R. D. *Organometallics* **1998**, *17*, 382. (b) Cuenca, T.; Royo, P. *J. Organomet. Chem.* **1985**, *293*, 61. (c) For related aluminum species see: Korolev, A. V.; Guzei, I. A.; Jordan, R. F. *J. Am. Chem. Soc*. **1999**, *121*, 11606.

(16) Howard, W. A.; Trnka, T. M.; Parkin, G. *Inorg. Chem.* **1995**, *34*, 5900.

(17) (a) Steffey, B. D.; Fanwick, P. E.; Rothwell, I. P. *Polyhedron* **1990**, *9*, 963. (b) Coffindaffer, T. W.; Steffy, B. D.; Rothwell, I. P.; Folting, K.; Huffman, J. C.; Streib, W. E. *J. Am. Chem. Soc.* **1989**, *111*, 4742.

(18) (a) Jordan, R. F. *Adv. Organomet. Chem.* **1991**, *32*, 325. (b) Guram, A. S.; Jordan, R. F. In *Comprehensive Organometallic Chemistry*; Lappert, M. F., Ed.; Pergamon: Oxford, UK, 1995; Vol. 4, pp 589−626. (c) Marks, T. J. *Acc. Chem. Res.* **1992**, *25*, 57. (d) Horton, A. D. *Trends Polym. Sci.* **1994**, *2*, 158. (e) Brintzinger, H. H.; Fischer, D.; Mulhaupt, R.; Rieger, B.; Waymouth, R. M. *Angew. Chem., Int. Ed. Engl.* **1995**, *34*, 1143. (f) Bochmann, M. *J. Chem. Soc., Dalton Trans.* **1996**, 255. (g) Kaminsky, W.; Arndt, M. *Adv. Polym. Sci.* **1997**, *127*, 143.

(19) Wu, Z.; Jordan, R. F.; Petersen, J. L. *J. Am. Chem. Soc.* **1995**, *117*, 5867.

(20) Carpentier, J.-F.; Maryin, V. P.; Luci, J.; Jordan, R. F., manuscript in preparation.

(21) (a) Stevens, J. C.; Timmers, F. J.; Rosen, G.; Knight, G. W.; Lai, S. Y. (Dow Chemical Co.). Eur. Patent Appl. EP 0416815 A2, 1991. (b) Canich, J. A. (Exxon Chemical Co.). Eur. Patent Appl. EP 0420436 A1, 1991. (c) McKnight, A. L.; Waymouth, R. M. *Chem. Rev.* **1998**, *98*, 2587.

(22) Use of $B(C_6F_5)_3$ for alkyl abstraction: (a) Yang, X.; Stern, C. L.; Marks, T. J. *J. Am. Chem. Soc.* **1994**, *116*, 10015 and references therein. (b) Ewen, J. A.; Elder, M. J. U.S. Patent Appl. 419,017, 1989; *Chem. Abstr*. **1991**, *115*, 136998g.

(23) The vinyl hydrogens are denoted according to

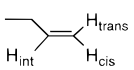

(24) However, J_{C-H} values are often insensitive to olefin coordination. See: Bender, B. R.; Norton, J. R.; Miller, M. M.; Anderson, O. P.; Rappé, A. K. *Organometallics* **1992**, *11*, 3427 and references therein.

Scheme 1

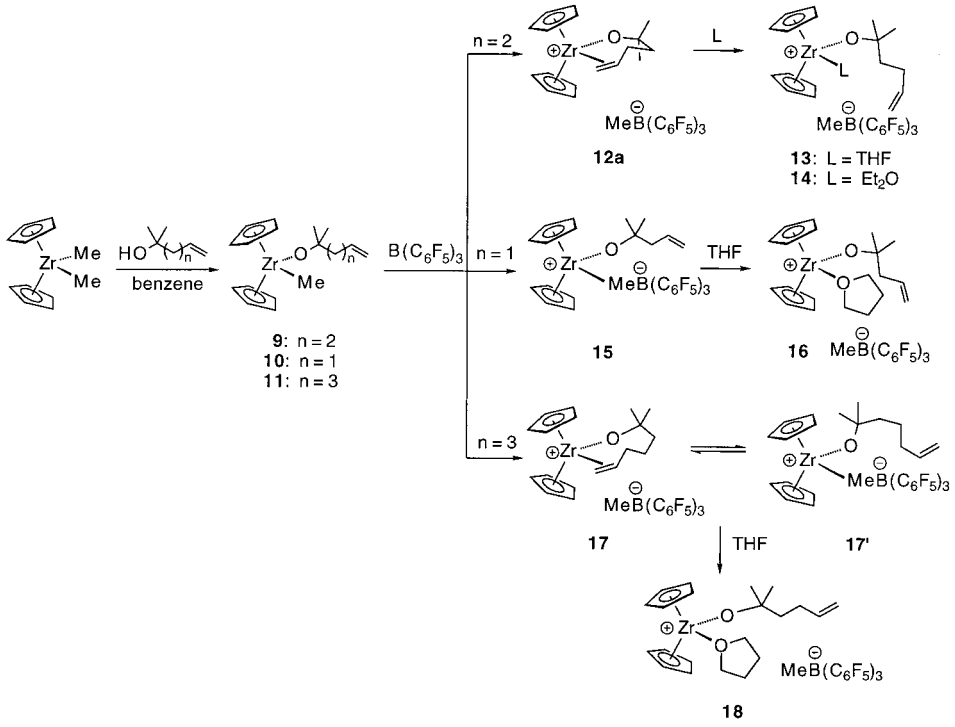

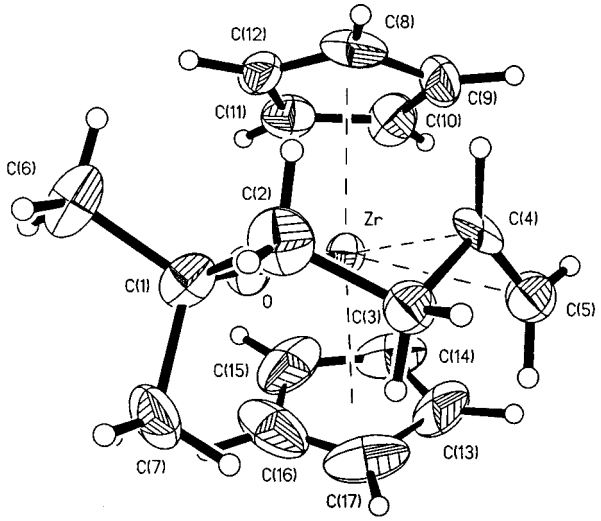

Figure 1. Molecular structure of the $(C_5H_5)_2Zr(OCMe_2CH_2CH_2CH{=}CH_2)^+$ cation.

communication.[19] The precision of this study was limited by a two-site conformational disorder involving the alkoxide ligand but is sufficient to confirm that the vinyl group is coordinated. Compound **12a** crystallizes as discrete ions. The structure of the $MeB(C_6F_5)_3^-$ anion is normal. The cation structure is shown in Figure 1. The pendant olefin group is coordinated to Zr in an unsymmetrical fashion, primarily through the terminal carbon ($Zr-C_{term}$ 2.68(2) Å, $Zr-C_{int}$ 2.89(2) Å). The coordinated olefin is tipped significantly from the O−Zr−(olefin centroid) plane (angle between planes Zr−C4−C5/O−Zr−(olefin centroid): 39.5° site 1; 25.3° site 2). The Zr−O distance (1.888(5) Å) and Zr−O−C angle (167.8(6)°) are very similar to those in the Cp_2-$Zr(O^tBu)(THF)^+$ cation (1.899(3) Å, 171.0(4)°).[25]

The $B(C_6F_5)_4^-$ salt **12b** was generated by the reaction of **9** with $[Ph_3C][B(C_6F_5)_4]$ in C_6D_6 (eq 2).[26] Salt **12b** separates from C_6D_6 as an orange oil but readily dissolves in CD_2Cl_2. The NMR data for **12b** in CD_2Cl_2 are identical to the data for **12a** with the exception of the anion resonances, confirming that ion pairing effects are minimal in this solvent.

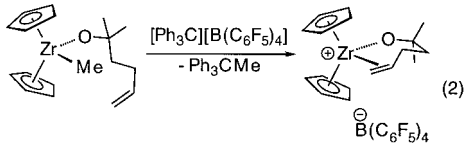

Reactions of $Cp_2Zr(OCMe_2CH_2CH_2CH{=}CH_2)^+$ with Lewis Bases. The reaction of **12a** with THF in CD_2Cl_2 solution results in displacement of the coordinated olefin and formation of THF adduct **13** (Scheme 1). The vinyl ^1H and ^{13}C NMR resonances of **13** are shifted back to the free olefin positions (cf. **9**), but the $MeB(C_6F_5)_3^-$ resonances are unchanged from those of **12a**. These observations confirm that the anion of **12a** is not coordinated in CD_2Cl_2. Similarly, addition of Et_2O to **12a** in CD_2Cl_2 solution yields ether adduct **14**. Addition of CO broadens but does not shift the resonances of **12a**, suggesting that CO binds reversibly to a small extent.[27] Addition of ethylene or 2-butyne has no effect on the NMR spectra of **12a**.

(25) (a) Collins, S.; Koene, B. E.; Ramachandran, R.; Taylor, N. J. *Organometallics* **1991**, *10*, 2092. For other $(C_5R_5)_2Zr(OR)(L)^+$ species see: (b) Jordan, R. F.; Dasher, W. D.; Echols, S. F. *J. Am. Chem. Soc.* **1986**, *108*, 1718.

(26) Use of $[Ph_3C][B(C_6F_5)_4]$ to generate zirconocene species: (a) Chien, J. C. W.; Tsai, W.-M., Rausch, M. D. *J. Am. Chem. Soc.* **1991**, *113*, 8570. (b) Ewen, J. A.; Elder, M. J. Eur. Patent Appl. 0,426,637, 1991; *Chem. Abstr.* **1991**, *115*, 136988d.

(27) For Zr^{IV} carbonyl complexes see: (a) Guram, A. S.; Swenson, D. C.; Jordan, R. F. *J. Am. Chem. Soc.* **1992**, *114*, 8991. (b) Antonelli, D. M.; Tjaden, E. B.; Stryker, J. M. *Organometallics* **1994**, *13*, 763. (c) Guo, Z. G.; Swenson, D. C.; Guram, A. S.; Jordan, R. F. *Organometallics* **1994**, *13*, 766. (d) Manriquez, J. M.; McAlister, D. R.; Sanner, R. D.; Bercaw, J. E. *J. Am. Chem. Soc.* **1978**, *100*, 2716. (e) Manriquez, J. M.; McAlister, D. R.; Sanner, R. D.; Bercaw, J. E. *J. Am. Chem. Soc.* **1976**, *98*, 6733. (f) Marsella, J. A.; Curtis, J. C.; Bercaw, J. E.; Caulton, K. G. *J. Am. Chem. Soc.* **1980**, *102*, 7244. (g) Howard, W. A.; Trnka, T. M.; Parkin, G. *Organometallics* **1995**, *14*, 4037. (h) Brakemeyer, T.; Erker, G.; Fröhlich, R. *Organometallics* **1997**, *16*, 531.

Solution Structures of $Cp_2Zr\{OCMe_2(CH_2)_nCH{=}CH_2\}^+$ (n = 1, 3) Species. The influence of the alkyl chain length on olefin binding in $Cp_2Zr\{OCMe_2(CH_2)_nCH{=}CH_2\}^+$ cations was probed by NMR studies of the reactions of **10** and **11** with $B(C_6F_5)_3$ (Scheme 1). Complex **10**, which contains a one-carbon spacer between the alkoxide and olefin groups, reacts with $B(C_6F_5)_3$ in CD_2Cl_2 solution to yield the ion pair $Cp_2Zr^{(+)}(OCMe_2CH_2CH{=}CH_2)(\mu\text{-Me})B^{(-)}(C_6F_5)_3$ (**15**, >95% NMR), in which the counterion rather than the olefin coordinates to Zr. The NMR resonances for the vinyl group of **15** are close to those of the free olefin and **10**, while the *Me*$B(C_6F_5)_3^-$ NMR resonances (B*Me*, 23 °C, CD_2Cl_2: ^{1}H NMR, δ 0.72; ^{13}C NMR, δ 2.7) are significantly shifted from the free anion positions. Addition of THF to a CD_2Cl_2 solution of **15** causes the *Me*$B(C_6F_5)_3^-$ resonances to shift to the free anion values, consistent with the formation of THF adduct **16**. The ^{1}H NMR spectrum of **16** (CD_2Cl_2) contains resonances for coordinated THF at δ 4.04 and 2.16.

In contrast, compound **11**, in which the alkoxide and vinyl functions are linked by a three-carbon tether, reacts with $B(C_6F_5)_3$ to yield a mixture of olefin adduct **17** and $MeB(C_6F_5)_3^-$ adduct **17′** (**17**/**17′** = 1.2/1 at −90 °C).[28] Cations **17**/**17′** have been characterized by low-temperature NMR but exchange rapidly on the NMR time scale at 23 °C. The NMR parameters for the coordinated olefin of **17** are nearly identical to the corresponding values for **12a**,**b**; in particular, the H_{int} resonance appears at low field (δ 7.40), the terminal vinyl ^{13}C resonance appears at high field (δ C_{term} 92.6), and the internal vinyl ^{13}C resonance appears at low field (δ C_{int} 157.9). The close similarity of the NMR data for the coordinated olefin groups in **12a**,**b** and **17** establishes that the metal−olefin bonding must be very similar in the two cations despite the difference in the length of alkyl tether that links the alkoxide and olefin functions, and implies that the chelation does not strongly perturb this bonding interaction. The reaction of **17**/**17′** with THF yields THF adduct **18** quantitatively.

Synthesis of *rac*-(EBI)Zr(OCMe$_2$CH$_2$CH$_2$CH=CH$_2$)$^+$. The reaction of *rac*-(EBI)$ZrMe_2$ (EBI = ethylene-1,2-bis(1-indenyl)) and 2-methyl-5-hexen-2-ol affords *rac*-(EBI)Zr($OCMe_2CH_2CH_2$-$CH{=}CH_2$)(Me) (**19**) in which the pendant olefin is not coordinated to Zr (eq 3).

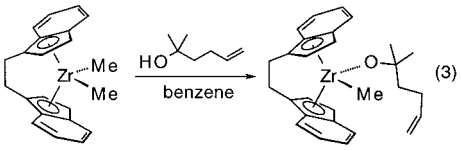

(3)

19

The reaction of **19** with $B(C_6F_5)_3$ in toluene cleanly yields [*rac*-(EBI)Zr($OCMe_2CH_2CH_2CH{=}CH_2$)][$MeB(C_6F_5)_3$] (**20a**) as a 1/1 mixture of diastereomers which differ in the relative configuration of the *rac*-(EBI)Zr unit and the internal carbon of the coordinated olefin (eq 4).[29] Compound **20a** separates from toluene as an orange oil but is soluble in chlorinated solvents. Recrystallization of **20a** from $CHCl_2CHCl_2$ affords the *S*,*S*,*R* (*ent* = *R*,*R*,*S*) diastereomer of **20a**·$CHCl_2CHCl_2$ as orange

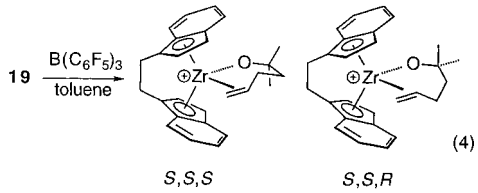

(4)

20a; anion = $Me\overset{\ominus}{B}(C_6F_5)_3$

crystals in 52% isolated yield (based on the 1/1 isomer ratio in solution). The presence of the solvent of crystallization in isolated **20a** was confirmed by NMR, elemental analysis, and an X-ray crystal structure determination (vide infra).

The *rac*-(EBI)Zr($OCMe_2CH_2CH_2CH{=}CH_2$)$^+$ cation (1/1 isomer mixture) was also generated as the $B(C_6F_5)_4^-$ salt (**20b**) on an NMR scale in C_6D_5Cl by the reaction of **19** with [Ph_3C]-[$B(C_6F_5)_4$] (eq 5). The ^{1}H NMR spectra of **20b** and **20a** are identical except for the anion resonance in the latter salt.

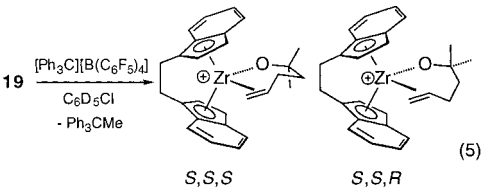

(5)

20b; anion = $\overset{\ominus}{B}(C_6F_5)_4$

Solid State Structure of [(*S*,*S*,*R*/*R*,*R*,*S*)-(EBI)Zr(OCMe$_2$-CH$_2$CH$_2$CH=CH$_2$)] [MeB(C$_6$F$_5$)$_3$] (20a). The solid-state molecular structure of **20a** (*S*,*S*,*R*/*R*,*R*,*S* isomer) was determined by X-ray diffraction (Figure 2, Tables 1 and 2). Complex **20a** crystallizes as discrete ions. The anion structure is normal. The structure of the (*S*,*S*,*R*/*R*,*R*,*S*)-(EBI)Zr($OCMe_2CH_2CH_2CH{=}CH_2$)$^+$ cation is similar to that of the $Cp_2Zr(OCMe_2CH_2CH_2$-$CH{=}CH_2)^+$ cation in **12a**. The olefin is coordinated to Zr primarily through the terminal carbon (Zr−C(26), 2.634(5); Zr−C(25), 2.819(4) Å). The Zr−C(26) distance is in the range observed for Zr−C_{sp^2} distances in other Zr^{IV} complexes of unsaturated π-systems, e.g., $(C_5R_5)_2Zr(\eta^2\text{-benzyl})(CH_3CN)^+$ complexes (Zr−C_{ipso}, 2.63−2.65 Å),[30] pentadienyl complex **5** (Zr−C_{sp2}, 2.66−2.76 Å),[9] $Cp_2Zr(\sigma^2,\pi\text{-diene})$ complexes (Zr−Cβ, 2.55−2.71 Å),[31] and the Zr^{IV} arene species $CpZr(CH_2Ph)_2$-$\{\eta^5\text{-PhCH}_2B(C_6F_5)_3\}$ (Zr−C_{Ph}, 2.65−2.76 Å) and $Zr(CH_2Ph)_3$-$\{\eta^6\text{-PhCH}_2B(C_6F_5)_3\}$ (Zr−C_{Ph}, 2.65−2.76 Å).[13g,h] These Zr^{IV}−C_{sp2} distances are all far longer than the Zr−C_{olefin} distances in Zr^{II} olefin complexes in which significant d−π* back-bonding is present, e.g., $Cp_2Zr(C_2H_4)(PMe_3)$ (2.354(3), 2.332(4) Å)[32] and $Cp_2Zr(\eta^2\text{-CH}_2{=}CHCH_2CH_3)(PMe_3)$ (2.357(9), 2.364(8) Å).[33] The Zr−C(25) distance in **20a** is beyond the limit where significant bonding interaction is expected.

The coordinated olefin of the (*S*,*S*,*R*/*R*,*R*,*S*)-(EBI)Zr($OCMe_2$-$CH_2CH_2CH{=}CH_2$)$^+$ cation is tipped significantly from the O−Zr−(olefin centroid) plane such that the angle between the

(28) The equilibrium constant for the **17** = **17′** equilibrium is given by K_{eq} = [**17′**]/{[$Cp_2Zr(OR)^+$][$MeB(C_6F_5)_3^-$]} = [**17′**]/[**17**]^2 = exp(−ΔG_{eq}/*RT*)). Thermodynamic parameters for the **17** = **17′** equilibrium were determined from K_{eq} values (Van't Hoff plot) in the range −90 to −30 °C: ΔH_{eq} = 0.9(4) kcal/mol, ΔS_{eq} = 12(2) eu. At 23 °C, K_{eq} = 88 M^{-1}.

(29) The isomers are denoted by the descriptors *S*,*S*,*S* (*ent* = *R*,*R*,*R*) and *S*,*S*,*R* (*ent* = *R*,*R*,*S*), in which the first two entries denote the configurations of the EBI bridgehead carbons and the third denotes that of C_{int} of the coordinated olefin.

(30) (a) Jordan, R. F.; LaPointe, R. E.; Bajgur, C. S.; Echols, S. F.; Willett, R. D. *J. Am. Chem. Soc.* **1987**, *109*, 4111. (b) Jordan, R. F.; LaPointe, R. E.; Baenziger, N. C.; Hinch, G. D. *Organometallics* **1990**, *9*, 1539.

(31) (a) Erker, G.; Wicher, J.; Engel, K.; Rosenfeldt, F.; Dietrich, W.; Krüger, C. *J. Am. Chem. Soc.* **1980**, *102*, 6346. (b) Krüger, C.; Müller, G.; Erker, G.; Dorf, U.; Engel, K. *Organometallics* **1985**, *4*, 215. (c) Yasuda, H.; Nakamura, A. *Angew. Chem., Int. Ed. Engl.* **1987**, *26*, 723.

(32) (a) Binger, P.; Muller, P.; Benn, R.; Rufinska, A.; Gabor, B.; Kruger, C.; Betz, P. *Chem. Ber.* **1989**, *122*, 1035. See also: (b) Alt, H. G.; Denner, C. E.; Thewalt, U.; Rausch, M. D. *J. Organomet. Chem.* **1988**, *356*, C83.

(33) Goddard, R.; Binger, P.; Hall, S. R.; Muller, P. *Acta Crystallogr., Sect. C* **1990**, *46*, 998.

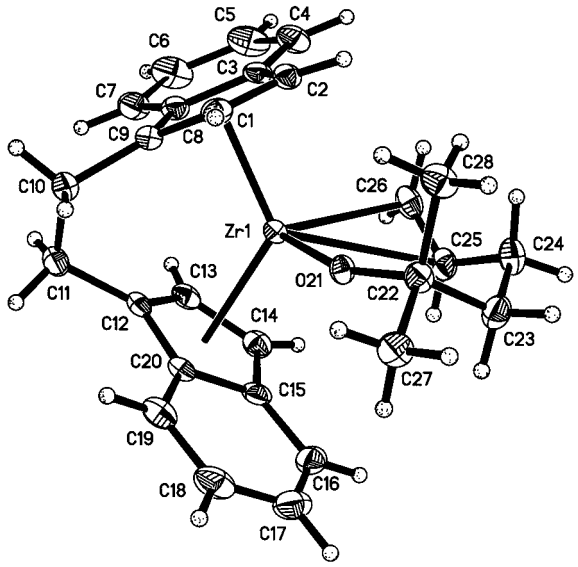

Figure 2. Molecular structure of the (*S,S,R*)-(EBI)Zr(OCMe$_2$CH$_2$CH$_2$-CH=CH$_2$)$^+$ cation.

Zr−C(25)−C(26) and O−Zr−(olefin centroid) planes is 31°. However, the olefin bonds to the metal in a "face-on" fashion; i.e., the dihedral angle between the plane of the olefin and the O−Zr−(olefin centroid) plane is 86.4°. The carbon and hydrogen atoms of the vinyl unit are coplanar to within 0.06 Å, and the C=C bond length (C(25)−C(26) = 1.325(8) Å) is not significantly perturbed from the value expected for a free α-olefin (1.335(5) Å).[34] In contrast, the olefin C−C distances in Cp$_2$Zr(C$_2$H$_4$)(PMe$_3$) (1.449(6) Å)[32] and Cp$_2$Zr(η^2-CH$_2$=CHCH$_2$CH$_3$)(PMe$_3$) (1.42(1) Å)[33] are lengthened about halfway toward the normal C−C single bond distance (1.537-(5) Å).

The Zr−O distance (1.897(3) Å) in **20a** is nearly equal to the corresponding distance in **12a**, while the Zr−O−C angle (159.7(3)°) is ca. 8° smaller than the corresponding angle in **12a**. For comparison, the Zr−O distance and Zr−O−C angles associated with the alkoxide ligand in *rac*-(EBTHI)Zr(O^{t}Bu)-(THF)$^+$ (EBTHI = ethylene-1,2-bis(tetrahydroindenyl)) are 1.929(3) Å and 161.9(4)° respectively.[35]

Solution Structure and NMR Assignments of 20a. The solution structure of **20a** was determined by 1D and 2D NMR studies. The ambient-temperature ^{1}H and ^{13}C NMR spectra of **20a** in CD$_2$Cl$_2$ and C$_6$D$_5$Cl solution contain two complete sets of resonances (the ^{1}H resonances are broadened by exchange, vide infra) and show that the two diastereomers are present in a 1/1 ratio and that isomer exchange is slow on the NMR chemical shift time scale under these conditions. The NMR data for **20a** are similar to the data for **12a**,**b** and establish that the olefin is coordinated to Zr in both isomers of **20a**. The vinyl C$_{term}$ ^{13}C NMR resonances (CD$_2$Cl$_2$) are shifted upfield (δ 99.9, 102.1), while the vinyl C$_{int}$ resonances are shifted downfield (δ 162.3, 164.7) from the corresponding resonances for the free olefin and **19** (δ 113.7, 140.1). Similarly, the vinyl ^{1}H resonances (C$_6$D$_5$Cl) are substantially shifted from those of the free olefin and **19**. In particular, the H$_{int}$ resonances appear at low field, δ 6.44 (*S,S,S* isomer) and δ 7.4−6.8 (*S,S,R* isomer, obscured by indenyl resonances). The *Me*B(C$_6$F$_5$)$_3^-$ ^{1}H NMR resonance appears at δ 1.18, which is characteristic of the free anion in C$_6$D$_5$Cl solvent (cf. [NBu$_3$CH$_2$Ph][MeB(C$_6$F$_5$)$_3$]: δ *Me*B = 1.11).

The low-temperature (−35 °C) ^{1}H NMR spectrum (C$_6$D$_5$Cl) of **20a** is sharp and contains two sets of vinyl resonances, four alkoxy methyl resonances (two for each isomer), and eight C$_5$-indenyl resonances (four for each isomer). The vinyl resonances

Table 1. Summary of Crystallographic Data for [*rac*-(EBI)Zr(OCMe$_2$CH$_2$CH$_2$CH=CH$_2$)][MeB(C$_6$F$_5$)$_3$]·CHCl$_2$CHCl$_2$ (**20a**·CHCl$_2$CHCl$_2$)

compound	**20a**·CHCl$_2$CHCl$_2$
empirical formula	C$_{48}$H$_{34}$BCl$_4$F$_{15}$OZr
formula weight	1155.6
temperature (K)	190
radiation	Mo Kα, 0.71073 Å
crystal size (mm)	0.38 × 0.32 × 0.22
crystal color/shape	red/irregular lath
crystal system	triclinic
space group	$P\bar{1}$
unit cell dimensions	a = 12.371(3) Å, α = 92.93(2)° b = 15.635(4) Å, β = 99.12(2)° c = 11.928(3) Å, γ = 99.44(2)°
volume (Å^3)	2240(2)
Z	2
D_{calcd} (g/cm^3)	1.71
absorption coefficient (cm^{-1})	5.80
2θ range (deg)	4.0 < 2θ < 55.0
index ranges	−16 ≤ h ≤ 16, −20 ≤ k ≤ 20, −15 ≤ l ≤ 6
reflections collected	14 598
independent reflections	10 188 (R_{int} = 0.032)
observed reflections	6289, $I > 2\sigma(I)$
structure solution	direct methods[a]
refinement method	full-matrix least squares vs F_o, all non-H anisotropic; H25, H26A, H26B isotropic, all other H included at calcd positions with $B_H = 1.2(B_{attached\ carbon})$[b]
total parameters	661
R	0.049[c]
R_w	0.061[d]
max. resid. density (e/Å^3)	1.01

[a] Main, P.; Fiske, S. J.; Hull, S. E.; Lessinger, L.; Germain, G.; DeClercq, J. P.; Woolfson, M. M. *Multan80*; University of York: York UK, 1980. [b] Data processing and refinement with MolEN: Fair, C. K. *An Interactive System for Crystal Structure Analysis*; Enraf Nonius: Delft, The Netherlands, 1990. [c] $R = \sum(|F_o| - |F_c|)/\sum F_o$. [d] $R_w = \{[\sum(F_o - F_c)^2]/[\sum w(F_o)^2]\}^{1/2}$.

Table 2. Selected Bond Lengths (Å) and Angles (deg) for [*rac*-(EBI)Zr(OCMe$_2$CH$_2$CH$_2$CH=CH$_2$)][MeB(C$_6$F$_5$)$_3$]·Cl$_2$CDCDCl$_2$ (**20a**·CHCl$_2$CHCl$_2$)[a]

Zr(1)−C(100)	2.229	Zr(1)−C(200)	2.248
Zr(1)−C(1)	2.442(4)	Zr(1)−C(2)	2.480(4)
Zr(1)−C(3)	2.638(4)	Zr(1)−C(8)	2.643(4)
Zr(1)−C(9)	2.473(4)	Zr(1)−C(12)	2.499(4)
Zr(1)−C(13)	2.502(4)	Zr(1)−C(14)	2.530(5)
Zr(1)−C(15)	2.639(4)	Zr(1)−C(20)	2.601(4)
Zr(1)−O(21)	1.897(3)	Zr(1)−C(26)	2.634(5)
Zr(1)−C(25)	2.819(4)	C(9)−C(10)	1.504(6)
C(11)−C(12)	1.504(6)	C(25)−C(26)	1.325(8)
C(24)−C(25)	1.495(7)	C(23)−C(24)	1.541(7)
C(22)−C(23)	1.523(7)	C(22)−O(21)	1.435(5)
C(100)−Zr(1)−C(200)	123.5	O(21)−Zr(1)−C(25)	69.1(2)
O(21)−Zr(1)−C(26)	92.6(2)	Zr(1)−O(21)−C(22)	159.7(3)
C(100)−Zr(1)−O(21)	113.1	C(200)−Zr(1)−O(21)	108.5
Zr(1)−C(26)−C(25)	83.9(3)	O(21)−C(22)−C(23)	106.5(3)
C(24)−C(25)−C(26)	125.4(5)	C(23)−C(24)−C(25)	114.2(4)
C(22)−C(23)−C(24)	114.4(4)	O(21)−C(22)−C(27)	108.3(4)
O(21)−C(22)−C(28)	108.8(4)		

[a] C(100) and C(200) denote the centroids of the five-membered rings of the indenyl groups.

(34) Gordon, A. J.; Ford, R. A. *The Chemist's Companion*; Wiley: New York, 1972; p 108.

(35) Hong, Y.; Kuntz, B. A.; Collins, S. *Organometallics* **1993**, *12*, 964.

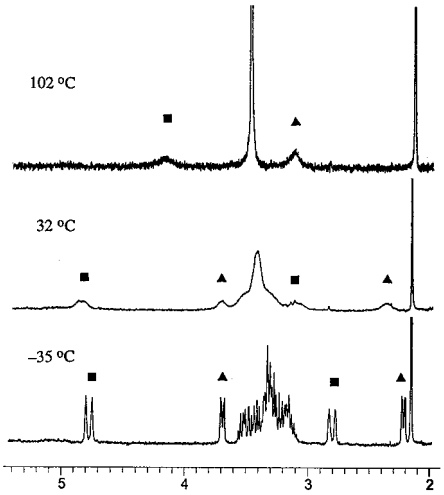

Figure 3. Vinyl region of the ^{1}H NMR spectra of **20a** (C_6D_5Cl). ■ = H_{trans}, ▲ = H_{cis}; specific isomer assignments are given in the text. The multiplet at δ 3.3 is due to the EBI ethylene bridge hydrogens, and the singlet at δ 2.14 is due to toluene which was added as a line width standard.

(Figure 3) were fully assigned by a combination of 2D COSY and NOESY spectra and chemical shift and J_{H-H} trends (see Experimental Section).[23] The H_{cis} resonance of the *S,S,S*/*R,R,R* isomer (δ 2.26, d, $^3J_{H-H}$ = 9 Hz) appears ca. 1.5 ppm upfield from the H_{cis} resonance of the *S,S,R*/*R,R,S* isomer (δ 3.71, d, $^3J_{H-H}$ = 9 Hz) due to anisotropic shielding by the C_6-indenyl ring. Similarly, the H_{trans} resonance for the *S,S,R* isomer (δ 2.80, d, $^3J_{H-H}$ = 18 Hz) appears ca. 2 ppm upfield of the H_{trans} resonance of the *S,S,S* isomer (δ 4.79, d, $^3J_{H-H}$ = 18 Hz). The alkoxide methyl groups that are syn (δ Me_{syn} 0.53, 0.27) and anti (δ Me_{anti} 0.70, 0.68) to the C_6-indenyl rings were identified from NOESY correlations; however, the Me_{syn} and Me_{anti} resonances could not be conclusively assigned to particular isomers.

Reaction of 20a with THF. The NMR results described above, and the fact that the NMR spectra of **20a** and **20b** are identical except for the anion resonances, establish that the pendant olefin in these species remains coordinated in C_6D_5Cl solution. This conclusion was confirmed by reaction of **20a** with THF (eq 6). This reaction yields the THF adduct [*rac*-(EBI)-$Zr(OCMe_2CH_2CH_2CH{=}CH_2)(THF)][MeB(C_6F_5)_3]$ (**21**) and causes the vinyl ^{1}H NMR resonances to shift to the free olefin positions, but does not affect the $MeB(C_6F_5)_3^-$ resonance.

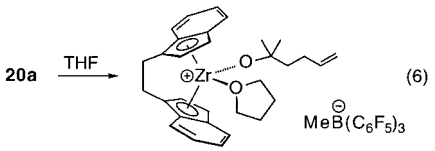

(6)

21

Dynamic Properties of $Cp_2Zr(OCMe_2CH_2CH_2CH{=}CH_2)^+$. As noted above, the low-temperature (−80 °C, CD_2Cl_2) ^{1}H NMR spectrum of the $Cp_2Zr(OCMe_2CH_2CH_2CH{=}CH_2)^+$ cation contains two singlets for the diastereotopic Cp groups and two singlets for the diastereotopic $ZrOCMe_2$ groups. These pairs of resonances each broaden and coalesce to a singlet at higher temperatures (T_{coal} = −65 °C for Cp, −55 °C for $ZrOCMe_2$ at 360 MHz). The dynamic process responsible for these line shape changes must involve inversion of configuration of the internal vinyl carbon, i.e., exchange of the olefin enantioface that is coordinated to Zr ("olefin face exchange"). The vinyl and

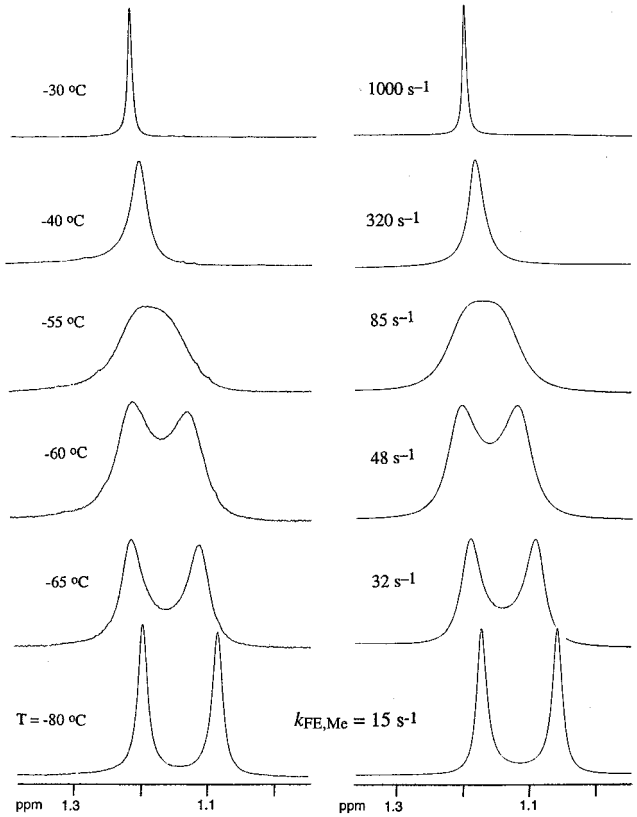

Figure 4. $ZrOCMe_2$ region of the ^{1}H NMR spectrum of **12b** (CD_2Cl_2). Experimental spectra are shown on the left, and simulated spectra are shown on the right. Best-fit first-order rate constants ($k_{FE,Me}$) are shown with the simulated spectra.

$MeB(C_6F_5)_3^-$ resonances do not shift significantly between −80 and 25 °C, which indicates that the extent of olefin dissociation is very minor (at best) in this temperature range.

The kinetics of $Cp_2Zr(OCMe_2CH_2CH_2CH{=}CH_2)^+$ face exchange were probed by line-shape analysis of the $ZrOCMe_2$ region of the −80 to −20 °C ^{1}H NMR spectra of **12b** in CD_2Cl_2 (Figure 4).[36] Spectra were simulated for a two-site system with equal populations, taking into account minor temperature variations of the chemical shifts (see Experimental Section). Exchange rates were obtained by comparison of experimental and simulated spectra. The activation parameters for the face exchange process determined from the Me exchange ($\Delta H^{\ddagger}_{FE,Me}$ = 9.6(5) kcal/mol; $\Delta S^{\ddagger}_{FE,Me}$ = −5(2) eu) were obtained from a standard least-squares Eyring analysis (Figure 5) according to eq 7, where $k_{FE,Me}$ is the first-order rate constant for face

$$\ln(k_{FE,Me}/T) = -\Delta H^{\ddagger}_{FE,Me}/(RT) + (\Delta S^{\ddagger}_{FE,Me}/R) + \ln(k_B/h) \quad (7)$$

exchange and k_B is the Boltzmann constant. The free energy of activation at the coalescence temperature calculated using these activation parameters (T_{coal} = −55 °C, $\Delta G^{\ddagger}_{FE,Me}$ = 10.7(5) kcal/mol) agrees well with the value ($\Delta G^{\ddagger}_{FE,Me}$ = 10.7(2) kcal/mol) estimated by eq 8 ($\Delta\nu$ = frequency difference at low-temperature limit) and eq 7.[37]

$$k_{coal} = \pi\Delta\nu/\sqrt{2} \quad (8)$$

Possible Mechanisms for Olefin Face Exchange. Four limiting mechanisms for "olefin face exchange" of a $(C_5R_5)_2Zr(OCMe_2CH_2CH_2CH{=}CH_2)^+$ cation are illustrated in Scheme 2. The simplest mechanism (i) involves simple olefin dissocia-

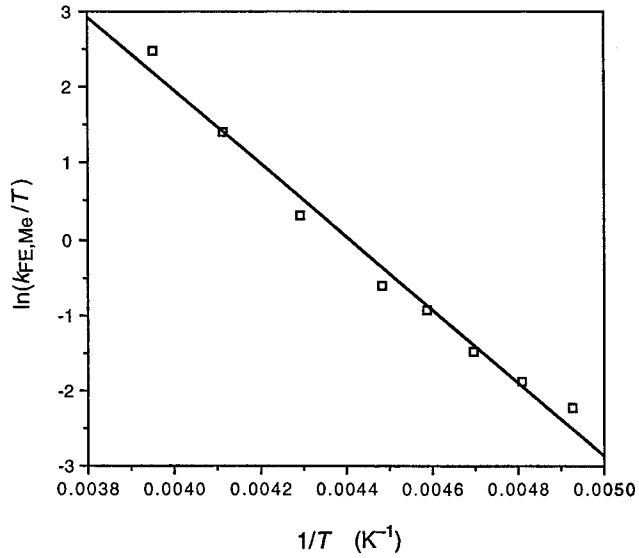

Figure 5. Eyring plot for ZrOC*Me*$_2$ exchange of **12b** (CD_2Cl_2 solvent) using the $k_{FE,Me}$ values.

Scheme 2

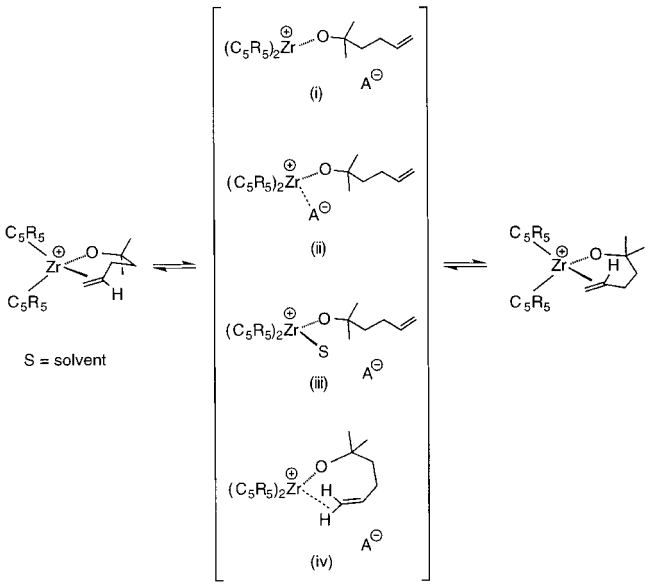

tion and recoordination through the opposite enantioface. Face exchange could also occur by associative processes in which the anion (ii) or solvent (iii) displaces the olefin. Alternatively, face exchange could occur by a "guided tour" mechanism (e.g., iv) involving a "σ-complex" intermediate in which the olefin remains weakly bonded to the metal center by a C−H−Zr agostic interaction. The metal can migrate back to either enantioface of the olefin as the σ-complex relaxes back to the π-complex. Mechanisms of this type have been proposed previously for the interconversion of diastereomeric CpRe(NO)-$(PPh_3)(CH_2{=}CHR)^+$ complexes.[38]

The ^{1}H NMR spectra of $MeB(C_6F_5)_3^-$ salt **12a** and $B(C_6F_5)_4^-$ salt **12b** are identical over the temperature range −80 to 25 °C (except for the anion resonances of **12a**), indicating that the dynamic properties of the $Cp_2Zr(OCMe_2CH_2CH_2CH{=}CH_2)^+$ cation are not influenced by these counterions. As $MeB(C_6F_5)_3^-$ is more strongly coordinating and nucleophilic than $B(C_6F_5)_4^-$, this result is strong evidence against the anion-assisted face exchange mechanism ii.[14] The data available for **12a** and **12b** do not allow mechanisms i, ii, and iv to be distinguished.[39] However, more extensive mechanistic information about the olefin face exchange for *rac*-(EBI)Zr$(OCMe_2CH_2CH_2CH{=}CH_2)^+$ is available as discussed below.

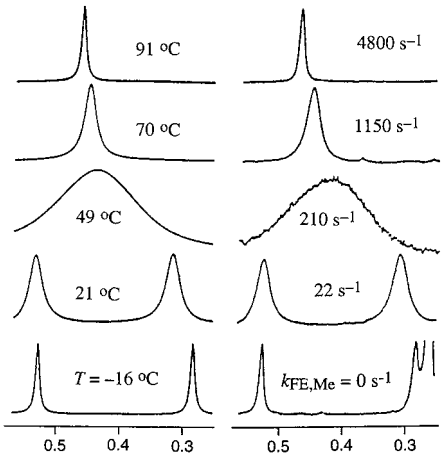

Figure 6. Me_{syn} region of the ^{1}H NMR spectra of **20a** (C_6D_5Cl). Experimental spectra are shown on the right, and simulated spectra are shown on the left. Best-fit first-order rate constants ($k_{FE,Me}$) are shown with the simulated spectra.

Dynamic Properties of *rac*-(EBI)Zr$(OCMe_2CH_2CH_2CH{=}CH_2)^+$. Variable-temperature ^{1}H NMR studies establish that **20a** also undergoes olefin face exchange, i.e., interconversion of the *S,S,R/R,R,S* and *S,S,S/R,R,R* isomers, on the NMR time scale. As illustrated in Figure 3, the pairs of H_{int}, H_{cis}, and H_{trans} ^{1}H NMR resonances of **20a** (corresponding to the two diastereomers) each collapse to a single resonance as the temperature is raised from −35 to 102 °C. Similarly, the pairs of Me_{syn} and Me_{anti} resonances each collapse to a singlet as the temperature is raised. The observation of *two* ZrOC*Me*$_2$ resonances at the high-temperature limit, i.e., the absence of Me_{syn}/Me_{anti} exchange, establishes that the alkoxide groups do not exchange between *rac*-(EBI)Zr units and implies that the face exchange process is intramolecular.[40]

(a) Me_{syn} Exchange. The kinetics of olefin face exchange for **20a** were first probed by line-shape analysis of the Me_{syn} region of the ^{1}H NMR spectra in the temperature range −16 to 91 °C in C_6D_5Cl (Figure 6).[41] Spectra were simulated for a two-site system with equal populations, corresponding to the 1/1 isomer ratio (see Experimental Section for details). The activation parameters for the face exchange determined from the Me_{syn} resonances ($\Delta H^{\ddagger}_{FE,Me}$ = 16.2(4) kcal/mol; $\Delta S^{\ddagger}_{FE,Me}$ = 3(2) eu)

(36) The ZrOC*Me*$_2$ region was selected for simulation because the chemical shift difference at the slow exchange limit is greater for the ZrOC*Me*$_2$ resonances than for the Cp resonances ($\Delta\delta$ = 0.115 and 0.035 respectively at −80 °C), which affords greater precision in the exchange rate determination. Simulation of the Cp resonances in the range −80 to −50 °C led to similar activation parameters.

(37) Sandström, J. *Dynamic NMR Spectroscopy*; Academic: London, 1982.

(38) (a) Peng, T.-S.; Gladysz, J. A. *J. Am. Chem. Soc.* **1992**, *114*, 4174. See also: (b) Kegley, S. E.; Walter, K. A.; Bergstrom, D. T.; MacFarland, D. K.; Young, B. G.; Rheingold, A. L. *Organometallics* **1993**, *12*, 2339. (c) Quirós-Méndez, N.; Mayne, C. L.; Gladysz, J. A. *Angew. Chem., Int. Ed. Engl.* **1990**, *29*, 1475.

(39) The solubility and reactivity properties of **12a**,**b** and the low face exchange barrier in this case limited dynamic NMR studies to CD_2Cl_2 solvent, so the influence of solvent properties could not be investigated conveniently.

(40) The ZrOC*Me*$_2$ groups are diastereotopic due to their proximity to the chiral *rac*-(EBI)Zr unit.

(41) The Me_{syn} region was selected for analysis because the difference in the chemical shifts ($\Delta\delta$ = 0.24) at the low-temperature limit (−16 °C) is greater than that for the Me_{anti} resonances ($\Delta\delta$ = 0.04), which results in greater precision in the exchange rate determination.

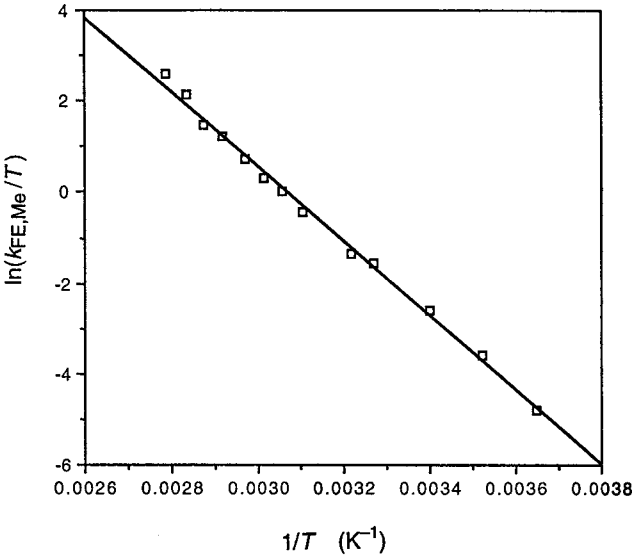

Figure 7. Eyring plot for Me_{syn} exchange of **20a** (C_6D_5Cl solvent) using the $k_{FE,Me}$ values.

were obtained by a standard Eyring analysis (Figure 7). The free energy of activation at the coalescence temperature calculated using these activation parameters ($\Delta G^{\ddagger}_{FE,Me} = 15.4(4)$ kcal/mol, $T_{coal} = 43$ °C) agrees well with the value estimated using eq 8 ($\Delta G^{\ddagger}_{FE,Me} = 15.3(2)$ kcal/mol).

(b) Anion and Solvent Participation. The most likely mechanisms for the *rac*-(EBI)Zr($OCMe_2CH_2CH_2CH{=}CH_2$)$^+$ face exchange are mechanisms i−iv in Scheme 2. Several observations show that the anion does not play a significant role the *rac*-(EBI)Zr($OCMe_2CH_2CH_2CH{=}CH_2$)$^+$ face exchange, and allow mechanism ii to be ruled out. The variable-temperature ^{1}H NMR spectra of $B(C_6F_5)_4^-$ salt **20b** are identical to those of $MeB(C_6F_5)_3^-$ salt **20a** over the range −50 to 60 °C, except for the anion resonances of **20a**.[42] Moreover, the ^{1}H NMR spectrum of **20a** at 62 °C is unchanged upon addition of excess $MeB(C_6F_5)_3^-$ (as $[NBu_3(CH_2Ph)][MeB(C_6F_5)_3]$).

It is more difficult to address the issue of solvent participation in the *rac*-(EBI)Zr($OCMe_2CH_2CH_2CH{=}CH_2$)$^+$ face exchange, because of the limited range of compatible solvents. However, the face exchange rates determined by line-shape analysis of the Me_{syn} region (and the C_5-indenyl region, vide infra) of the ^{1}H NMR spectra of **20a** in CD_2Cl_2 agree well with the values determined in C_6D_5Cl over the temperature range −8 to 23 °C. Additionally, the free energy barrier for olefin face exchange determined from coalescence of the Me_{syn} resonances in CD_2Cl_2 ($\Delta G^{\ddagger}_{FE,Me} = 15.3(2)$ kcal/mol, $T_{coal} = 23$ °C) is identical to that determined in C_6D_5Cl ($\Delta G^{\ddagger}_{FE,Me} = 15.3(2)$ kcal/mol, $T_{coal} = 43$ °C). The similarity of the dynamic behavior of **20a** in C_6D_5Cl and CD_2Cl_2 and the near-zero value for $\Delta S^{\ddagger}_{FE,Me}$ for **20a** suggest that solvent assistance does not play an important role in the olefin face exchange of this compound.[43] However, it should be pointed out that little is known about the relative coordinating ability or nucleophilicity of different chlorocarbon solvents.[44,45] Crabtree has reported that addition of 1 equiv of chlorobenzene to $(cod)Ir(PMePh_2)_2^+$ (cod = cyclooctadiene) inhibits Ir-catalyzed cyclohexene hydrogenation in methylene chloride solvent.[46] This effect was ascribed to the formation of $IrH_2(PMePh_2)_2(chlorobenzene)_2^+$ and suggests that chlorobenzene is a significantly stronger ligand for Ir^{III} than is methylene chloride. While a chlorobenzene adduct has not yet been isolated in this system, the chelated species $Ir(cod)\{\eta^2\text{-}PPh_2(o\text{-}C_6H_4Cl)\}^+$ has been characterized.[47] On the other hand, Gladysz et al. have identified the dichloromethane complex $[(\eta^5\text{-}C_5Me_5)Re(NO)(PPh_3)(ClCH_2Cl)][BF_4]$ and the analogous chlorobenzene complex $[(\eta^5\text{-}C_5Me_5)Re(NO)(PPh_3)(ClC_6H_5)]BF_4]$.[48] ^{31}P NMR experiments show that treatment of the latter species with CH_2Cl_2 converts it to the CH_2Cl_2 complex, indicating that CH_2Cl_2 is a stronger ligand than C_6H_5Cl for the $(\eta^5\text{-}C_5Me_5)Re(NO)(PPh_3)^+$ cation.

Scheme 3

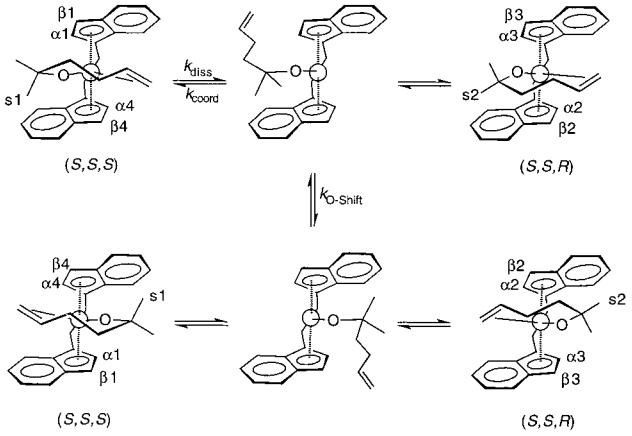

(c) Differentiation of Dissociative and Nondissociative Face Exchange Mechanisms. The two remaining possible face exchange mechanisms for *rac*-(EBI)Zr($OCMe_2CH_2CH_2CH{=}CH_2$)$^+$, i.e., olefin dissociation/recoordination (process i in Scheme 2) and the nondissociative σ-complex mechanism (process iv in Scheme 2) are illustrated in more detail in Schemes 3 and 4. As is evident from Scheme 4, in the

(42) The free energy barrier for olefin face exchange determined from coalescence of the Me_{syn} resonances for **20b** ($\Delta G^{\ddagger}_{FE,Me} = 15.4(2)$ kcal/mol) is identical to that determined for **20a**.

(43) Purely associative mechanisms are generally characterized by $\Delta S^{\ddagger}$ values below −10 eu. However, activation entropies are difficult to determine precisely and must be interpreted carefully because of possible contributions from solvent reorganization, especially for polar solvents and charged metal complexes. See: (a) Atwood, J. D. *Inorganic and Organometallic Reaction Mechanisms*; Brooks/Cole: Monterey, CA, 1985; p 17. (b) Jordan, R. B. *Reaction Mechanisms of Inorganic and Organometallic Systems*; Oxford University: New York, 1991; pp 56−57.

(44) (a) Beck, W.; Schloter, K. Z. *Z. Naturforsch.* **1978**, *33B*, 1214. (b) Sünkel, K.; Urban, G.; Beck, W. *J. Organomet. Chem.* **1983**, *252*, 187. (c) Fernandez, J. M.; Gladysz, J. A. *Organometallics* **1989**, *8*, 207. (d) Kulaviec, R. J.; Crabtree, R. H. *Coord. Chem. Rev.* **1990**, *99*, 89. (e) Bown, M.; Waters, J. M. *J. Am. Chem. Soc.* **1990**, *112*, 2442. (f) Colsman, M. R.; Newbound, T. D.; Marshall, L. J.; Noirot, M. D.; Miller, M. M.; Wulfberg, G. P.; Frye, J. S.; Anderson, O. P.; Strauss, S. H. *J. Am. Chem. Soc.* **1990**, *112*, 2349. (g) Van Seggen, D. M.; Anderson, O. P.; Strauss, S. H. *Inorg. Chem.* **1992**, *31*, 2987. (h) Woska, D. C.; Wilson, M.; Bartholomew, J.; Eriks, K.; Prock, A.; Giering, W. P. *Organometallics* **1992**, *11*, 3343. (i) Seligson, A. L.; Trogler, W. C. *Organometallics* **1993**, *12*, 738. (j) Arndtsen, B. A.; Bergman, R. G. *Science* **1995**, *270*, 1970. (k) Forniés, J.; Martinez, F.; Navarro, R.; Urriolabeitia, E. P. *Organometallics* **1996**, *15*, 1813. (l) Butts, M. D.; Scott, B. L.; Kubas, G. J. *J. Am. Chem. Soc.* **1996**, *118*, 11831. (m) Huhmann-Vincent, J.; Scott, B. L.; Kubas, G. J. *J. Am. Chem. Soc.* **1998**, *120*, 6808. (n) Huang, D.; Huffman, J. C.; Bollinger, J. C.; Eisenstein, O.; Caulton, K. G. *J. Am. Chem. Soc.* **1997**, *119*, 7398.

(45) (a) The ionization energies of chlorobenzene (11.4 eV) and dichloromethane (11.35 eV) are similar. See: Debies, T. P.; Rabalais, J. W. *J. Electron Spectrosc.* **1972**, *1*, 355. Werner, A. S.; Tsai, B. P.; Baer, T. *J. Chem. Phys.* **1974**, *60*, 3650. (b) The dielectric constant (ϵ, 20 °C) of dichloromethane (9.08) is greater thatn that of chlorobenzene (5.71). *CRC Handbook of Chemistry and Physics*; Weast, R. C., Astle, M. J., Eds.; CRC: Boca Raton, FL, 1982; p E-51.

(46) Crabtree, R. H.; Demou, P. C.; Eden, D.; Mihelcic, J. M.; Parnell, C. A.; Quirk, J. M.; Morris, G. E. *J. Am. Chem. Soc.* **1982**, *104*, 6994.

(47) Burk, M. J.; Crabtree, R. H.; Holt, E. M. *Organometallics* **1984**, *3*, 638.

(48) (a) Kowalczyk, J. J.; Agbossou, S. K.; Gladysz, J. A. *J. Organomet. Chem.* **1990**, *397*, 333. (b) Peng, T.-S.; Winter, C. H.; Gladysz, J. A. *Inorg. Chem.* **1994**, *33*, 2534. (c) Szafert, S.; Gladysz, J., private communication.

Scheme 4

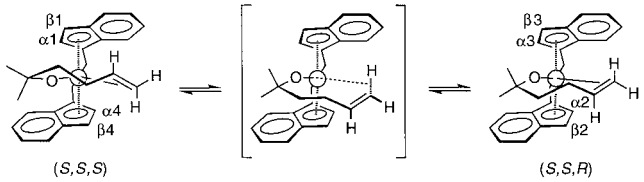

σ-complex mechanism, the face exchange does not permute the two indenyl rings of a given (EBI)Zr unit, and at the high-temperature limit *four* C_5-indenyl ^{1}H NMR resonances (two α and two β; vs ethylene bridge) should still be observed. In contrast, if complete olefin dissociation occurs (Scheme 3), an "O-shift" process in which the alkoxide ligand moves between the lateral coordination sites is possible. The O-shift permutes the two indenyl rings of a given (EBI)Zr unit. If the olefin face exchange is accompanied by the O-shift, the eight C_5-indenyl ^{1}H NMR resonances will collapse to *two* resonances at the high-temperature limit. The O-shift barrier should be low for a base-free $(C_5R_5)_2Zr(OR)^+$ cation because the alkoxide ligand is expected to occupy the central coordination site in the ground-state structure to maximize Zr−O π-bonding and minimize steric interactions.[49,50] It is important to note that the O-shift cannot occur if the olefin remains coordinated. Thus, while it is difficult to predict the relative rates at which the η^1-alkoxide intermediate would collapse back to the π-complex or undergo the O-shift, the detection of any leakage of the system through the O-shift is strong evidence for a dissociative face exchange.

(d) C_5-Indenyl H_α and H_β Exchanges. The C_5-indenyl region of the ^{1}H NMR spectra of **20a** in C_6D_5Cl over the temperature range −13 to 87 °C is shown in Figure 8. The four pairs of H_α and H_β resonances corresponding to the hydrogens on a given C_5-indenyl ring were identified from COSY correlations. The four H_α resonances (δ H_α at −13 °C: 6.01, 5.72, 5.70, and 5.63) were identified by NOESY correlations with the ethylene bridge hydrogens; the remaining four C_5-indenyl resonances are assigned to H_β (δ H_β at −13 °C: 5.81, 5.79, 5.78, and 5.68). It was not possible to conclusively assign all of the C_5-indenyl resonances to particular isomers (see Experimental Section for partial assignment). As the temperature is raised to the high-temperature limit, the eight C_5-indenyl resonances (four H_α and four H_β) collapse to two resonances (one H_α and one H_β; Figure 8). In addition, the 2D ^{1}H-EXSY spectrum of **20a** at −16 °C exhibits cross-peaks between each H_α resonance and the other three H_α resonances, and between each H_β resonance and the other three H_β resonances, showing that each H_α exchanges with the other three H_α's and each H_β exchanges with the other three H_β's. These observations establish that **20a** undergoes the O-shift process on the chemical shift time scale at high temperature and on the T_1 time scale at low temperature, which in turn means that olefin dissociation also occurs on these time scales. These qualitative observations provide strong evidence for a dissociative mechanism for olefin face exchange of *rac*-(EBI)Zr$(OCMe_2CH_2CH_2CH{=}CH_2)^+$ as outlined in Scheme 3, but do not rule out a partial contribution from a competing σ-complex mechanism (Scheme 4). To address this issue, we performed a detailed line-shape analysis of the C_5-indenyl region.

The H_α exchange system comprises four sites which are labeled α1, α2, α3, and α4 in Scheme 3. Sites α1 and α4 correspond to the H_α's of the *S,S,S/R,R,R* diastereomer, and sites α2 and α3 correspond to the H_α's of the *S,S,R/R,R,S* diastereomer. Because the isomer ratio is 1/1, the relative populations (mole fractions) of sites α1, α2, α3, and α4 are 1/4 each. Similarly, the H_β exchange system comprises four sites, which are labeled β1, β2, β3, and β4 in Scheme 3. The relative populations (mole fractions) of sites β1, β2, β3, and β4 are 1/4 each. The existence of four α and four β sites implies the existence of two sets of six possible site-to-site exchanges (α1−α2, α1−α3, α1−α4, α2−α3, α2−α4, α3−α4; β1−β2, β1−β3, β1−β4, β2−β3, β2−β4, β3−β4). Assuming that (i) olefin face exchange occurs by olefin dissociation/recoordination and (ii) the O-shift is much faster than olefin recoordination, i.e., $k_{OS} \gg k_{coord}$ in Scheme 3, then exchange of the four H_α's and exchange of the four H_β's will proceed statistically, according to the relative populations of the different sites. The rate for each site-to-site exchange is given by eq 9, in which p_{ij} is the

$$R_{ij} = p_{ij}P_ik \tag{9}$$

probability of exchanging from site *i* to site *j*, P_i is the population of site *i*, and *k* is defined in terms of the mean lifetime τ of all sites by $k = 1/\tau$.[51] As the four α and the four β sites are equally populated (i.e., $P_i = 1/4$) and the probability of exchanging from site *i* to *j* is the same for the two sets of six exchanges (i.e., $p_{ij} = 1/4$), all possible site-to-site exchanges should occur at the same rate, i.e.

$$R_{\alpha_i\alpha_j} = R_{\beta_i\beta_j} = k(1/4)(1/4) \tag{10}$$

On the other hand, if σ-complexes were involved or if the O-shift were not much faster than olefin recoordination, then the site-to-site exchange rates ($R_{\alpha_i\alpha_j}$) would not be equal; rather, the exchanges that require and O-shift (α1−α2, α1−α4, α2−α3, α3−α4; β1−β2, β1−β4, β2−β3, β3−β4) would occur at slower rates (R_{OS}) than those that do not (α1−α3, α2−α4; β1−β3, β2−β4; R_{no-OS}). Accordingly, the spectra were simulated for different ratios of R_{OS}/R_{no-OS}. The spectrum at 12 °C (intermediate exchange region) proved to be the most sensitive to the simulation parameters. At this temperature it was found that a ratio $R_{OS}/R_{no-OS} = 1/1 \pm 30\%$ was required to obtain satisfactory agreement between the observed and calculated spectra. This result supports the dissociative mechanism (i) for face exchange of **20a**.[52] A comparison between the experimental spectra and spectra simulated assuming that all $R_{\alpha_i\alpha_j}$ and $R_{\beta_i\beta_j}$ values are equal is shown in Figure 8.

At this stage it is useful to relate the rate constants for (a) the H_α site-to-site exchanges ($k_{\alpha_i\alpha_j}$), (b) olefin face exchange

(49) Examples of structurally characterized d^0 $(C_5R_5)_2MX$ compounds are given in the literature. (a) $(C_5Me_5)_2Sm(THF)$: Evans, W. J.; Kociok-Kohn, G.; Foster, S. E.; Ziller, J. W.; Doedens, R. J. *J. Organomet. Chem.* **1993**, *444*, 61. (b) $[(C_5Me_5)_2Sm]_2(\mu\text{-}O)$: Evans, W. J.; Grate, J. W.; Bloom, I.; Hunter, W. E.; Atwood, J. L. *J. Am. Chem. Soc.* **1985**, *107*, 405. (c) $(C_5Me_5)_2Sm(O\text{-}2,3,5,6\text{-}Me_4\text{-}Ph)$: Evans, W. J. *Inorg. Chim. Acta* **1985**, *110*, 191. (d) $(C_5Me_5)_2ScMe$: Thompson, M. E.; Baxter, S. M.; Bulls, A. R.; Burger, B. J.; Nolan, M. C.; Santarsiero, B. D.; Schafer, W. P.; Bercaw. J. E. *J. Am. Chem. Soc.* **1987**, *109*, 203. (e) See also: $(C_5Me_5)(\eta^5\text{-}C_2H_9H_{11})$-Ti(N=$CMe_2$): Kreuder, C.; Zhang, H.; Jordan, R. F. *Organometallics* **1995**, *14*, 2993.

(50) The O-shift barrier might be higher if the cation is strongly solvated or the anion strongly coordinates.

(51) (a) Perrin, C. L.; Dwyer, T. J. *Chem. Rev.* **1990**, *90*, 935. See also: (b) Orrell, K. G.; Sik, V. Dynamic NMR Spectroscopy in Inorganic and Organometallic Chemistry. In *Annual Reports in NMR Spectroscopy*; Webb, G. A., Ed.; Academic: New York, 1993; Vol. 27, pp 103−172.

(52) (a) However, because of the range of R_{OS}/R_{no-OS} ratios that provide satisfactory agreement between observed and simulated spectra ($R_{OS}/R_{no-OS} = 1/1 \pm 30\%$), a minor contribution from a nondissociative σ-complex intermediate cannot be definitively ruled out. (b) This degree of precision in the determination of exchange rates is typical for NMR simulations of this type. (c) This simulation problem is complicated by the small chemical shift difference between the resonances and by the temperature variation of the chemical shifts.

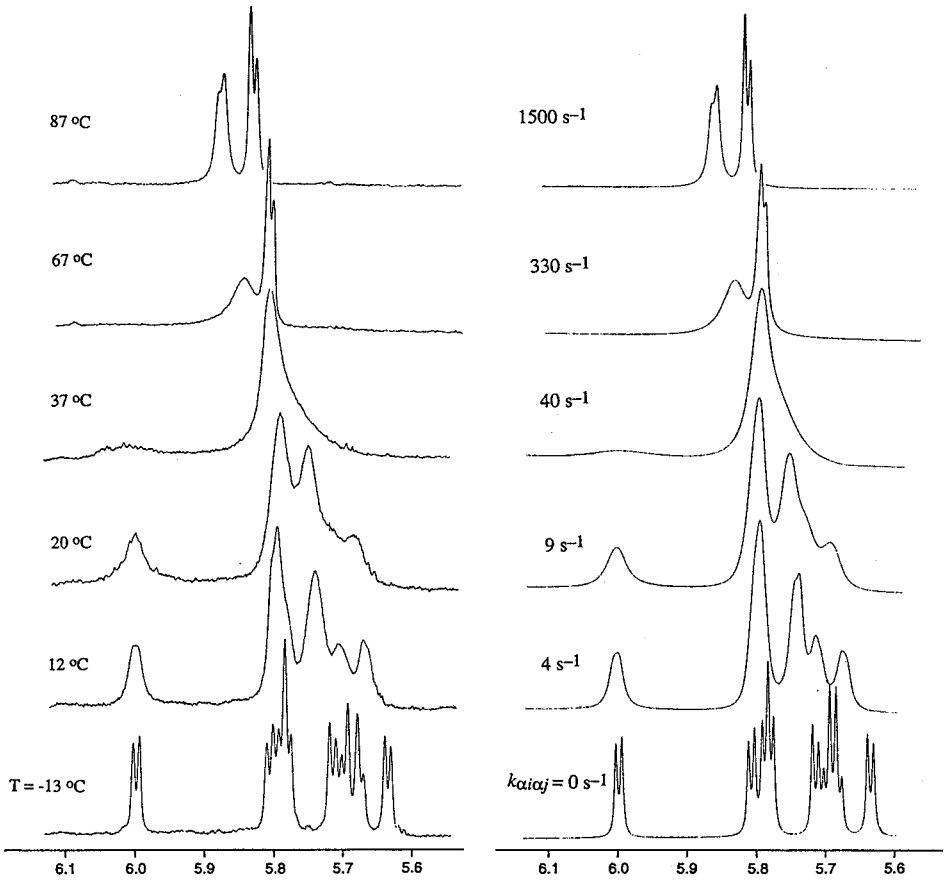

Figure 8. C_5-indenyl region of the ^{1}H NMR spectra of **20a** (C_6D_5Cl). Experimental spectra are shown on the left and simulated spectra are shown on the right. Best-fit first-order rate constants ($k_{\alpha_i\alpha_j}$) are shown with the simulated spectra.

determined from analysis of the Me_{syn} region ($k_{FE,Me}$), and (c) dissociation of the olefin (k_{diss}). As is evident from Scheme 3, if assumptions i and ii above are correct, a given H_α exchanges with each of the other three H_α's in one out of four olefin dissociation events, i.e.,

$$k_{\alpha_i\alpha_j} = k_{diss}/4 \tag{11}$$

Similarly, a given Me_{syn} group exchanges with the other Me_{syn} group in one out of two dissociation events, i.e.,

$$k_{FE,Me} = k_{diss}/2 \tag{12}$$

Therefore, it is expected that

$$2k_{\alpha_i\alpha_j} = k_{FE,Me} \tag{13}$$

Accordingly, the values of $2k_{\alpha_i\alpha_j}$ were used in an Eyring analysis (Figure 9) to calculate the activation parameters for the olefin face exchange determined by the H_α simulation ($\Delta H^{\ddagger}_{FE,\alpha}$ = 15.5(6) kcal/mol; $\Delta S^{\ddagger}_{FE,\alpha}$ = 0(2) eu).[53] These values agree within experimental uncertainty with those determined by the Me_{syn} simulation.

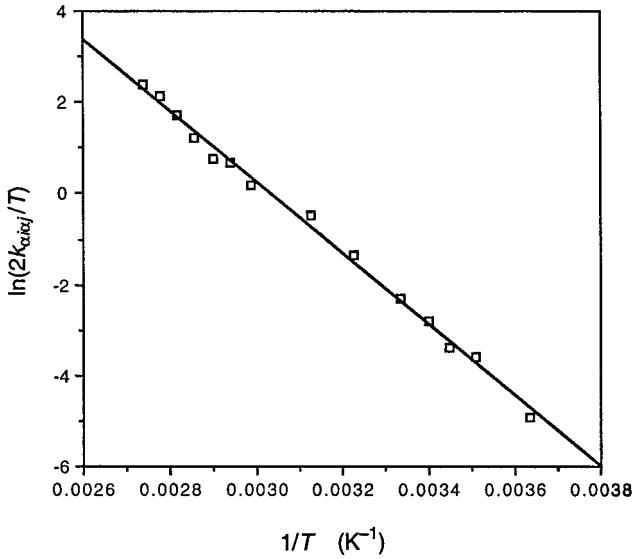

Figure 9. Eyring plot for C_5-indenyl exchange of **20a** (C_6D_5Cl solvent). The exchange rate constant $k_{FE,Me} = 2k_{\alpha_i\alpha_j}$.

In summary, the following key results emerge from our study of the dynamic properties of *rac*-(EBI)Zr($OCMe_2CH_2CH_2CH{=}CH_2$)$^+$: (i) the alkoxide ligand does not exchange between *rac*-(EBI)Zr units, which implies that the olefin face exchange is intramolecular; (ii) the dynamic properties are not influenced by the counterion, which implies that the face exchange is not assisted by the anion; (iii) the C_5-indenyl H_α and H_β exchanges are statistical and the activation parameters for the Me_{syn}

(53) The vinyl region of the ^{1}H NMR spectra of **20a** was also simulated. This subspectrum was simulated as an ensemble of three two-site equal-population exchange systems, corresponding to the pairs of H_{int}, H_{trans}, and H_{cis}. The face exchange rate constants determined for the Me_{syn} and H_α simulations ($k_{FE,Me} = 2k_{\alpha_i\alpha_j}$) were used as the exchange rate constants for each of the two-site systems. Satisfactory agreement between observed and simulated spectra was obtained for temperatures below 32 °C and above 92 °C (the spectra between 32 and 92 °C are too featureless to simulate). This result confirms that the vinyl group undergoes face exchange as a unit and supports the dissociative/fast O-shift mechanism. This simulation also showed that the coalesced resonances for H_{trans} and H_{cis} will become sharp only above ca. 130 °C (see Figure 3).

exchange and the H_α and H_β exchanges agree within experimental uncertainty, which implies that the face exchange is accompanied by fast O-shift and that nondissociative olefin face exchange via σ-complex intermediates is not important in this system.[52] These results are best accommodated by Scheme 3, in which the rate-limiting step is olefin dissociation. The activation parameters for olefin dissociation of **20a** are $\Delta H^{\ddagger}_{diss}$ = 15.8(6) kcal/mol, $\Delta S^{\ddagger}_{diss}$ = 2(2) eu.[54] It is possible that the solvent assists the olefin dissociation and stabilizes the nonchelated intermediate, but the similar dynamic behavior in CD_2Cl_2 and C_6H_5Cl and the near-zero $\Delta S^{\ddagger}_{FE}$ value argue against significant solvent participation.

Discussion

X-ray diffraction and NMR spectroscopic studies establish that the $Cp_2Zr(OCMe_2CH_2CH_2CH{=}CH_2)^+$ and *rac*-(EBI)Zr$(OCMe_2CH_2CH_2CH{=}CH_2)^+$ cations adopt chelated structures in the solid state and in CD_2Cl_2 and C_6D_5Cl solution. Thus these cations are rare examples of isolable d^0 metal olefin complexes. In this section we discuss the nature of the Zr−olefin bonding in these complexes and implications for the structures and reactivity of d^0 metal olefin complexes in general.

Utility of $(C_5R_5)_2Zr(OCMe_2CH_2CH_2CH{=}CH_2)^+$ Complexes as Models for $(C_5R_5)_2Zr(R)(olefin)^+$ Species. As noted in the Introduction, $(C_5R_5)_2Zr(R)(olefin)^+$ olefin adducts (**8**) are of particular interest because of their role as key intermediates in metallocene-catalyzed olefin polymerization. Before discussing the bonding in model complexes **7** and possible implications for the properties of **8**, it is useful first to comment on the differences between **7** and **8** and the extent to which these differences might influence the geometry of the Zr−olefin unit and the strength of the Zr−olefin bond. The model species **7** differ from **8** in two key respects: (i) in **7** the olefin is incorporated into a chelate ring and (ii) **7** contains a Zr−OR alkoxide ligand in place of the Zr−R alkyl ligand of **8**.

Several observations indicate that the chelate rings in **7** are sufficiently flexible that the Zr−olefin bonding is not significantly constrained by the chelation. (i) The ^{1}H and ^{13}C NMR data for the coordinated olefin groups in **12a**,**b** and **17** are nearly identical. This result establishes that the metal-olefin bonding must be very similar in the two compounds, despite the difference in chelate ring size, and implies that the chelation does not strongly perturb this bonding interaction. (ii) The chelate ring in **12a** is disordered between two conformations in the solid state, consistent with a high degree of flexibility. (iii) The structural and NMR spectroscopic parameters for the metal−olefin units in **12a**,**b** and **20a**,**b** are very similar despite the difference in metallocene structure. Furthermore, as will be discussed in the following paper in this series, the NMR data for the olefin units in $\{\eta^5{:}\eta^1\text{-}C_5R_4SiMe_2N^tBu\}Ti(OCMe_2CH_2CH_2CH{=}CH_2)^+$ cations (R = H, Me) are very similar to the data for **12a**,**b** and **20a**,**b**, despite the difference in metal and ancillary ligands.[20] The apparent lack of change in the metal−olefin bonding in response to changes in ancillary ligand structure, M−O−C bond distances and angles, and M−C distances is consistent with flexible chelate structures and relatively unconstrained metal−olefin bonding.

Replacement of the alkyl ligand in **8** with the alkoxide ligand in **7** is expected to decrease the Lewis acidity of the $(C_5R_5)_2ZrX^+$ unit due to O−Zr π-donation. While studies of the relative Lewis acidity of $(C_5R_5)_2ZrR^+$ and $(C_5R_5)_2Zr(OR)^+$ cations have not been reported, alkoxide π-donation is known to reduce the Lewis acidity of related four-coordinate metallocene species and main group Lewis acids. For example, associative THF exchange is significantly faster for $Cp_2Zr(Me)(THF)^+$ than for $Cp_2Zr(O^tBu)(THF)^+$,[25] Cp_2ZrMe_2 undergoes facile carbonylation to $Cp_2Zr\{\eta^2\text{-}C(=O)Me\}Me$ while $Cp_2Zr(Me)(OEt)$ does not,[55] and BR_3 alkyls are much stronger Lewis acids than are $B(OR)_3$ alkoxides.[56] Thus, the Zr−olefin bond in **7** is probably somewhat weaker than those in comparable alkyl analogues.

Metal−Olefin Bonding in $(C_5R_5)_2Zr(OCMe_2CH_2CH_2CH{=}CH_2)^+$ Cations. The X-ray structural analyses of **12a** and **20a** establish that the Zr−olefin bonding in these complexes is very unsymmetrical. The Zr−C_{term} contacts (2.63−2.68 Å) are in the range observed for the weak Zr−C interactions in Zr^{IV} π-complexes (e.g., η^2-benzyl or diene complexes) and in β-agostic species (e.g., $(C_5H_4Me)_2Zr(CH_2CH_3)(PMe_3)^+$ or $(C_5H_4Me)_2Zr(CH_2CH_2SiMe_3)(THF)^+$).[57] The Zr−$C_{int}$ distances are much longer (>2.82 Å) and indicate that there is no significant bonding interaction between these atoms.

The X-ray data for **20a** (C=C distance unchanged from free olefin value; vinyl carbons and hydrogens coplanar), the IR data for **12a** ($\nu_{C=C}$ unchanged from free olefin value), and the vinyl J_{CH} values for **12a** and **20a** (unchanged from free olefin values) collectively establish that the structure of the olefin unit is not significantly perturbed upon coordination in these systems. However, the divergence of the vinyl ^{13}C chemical shifts from the free olefin values, i.e., the ca. 20 ppm *upfield* shift of the C_{term} resonance and the ca. 20 ppm *downfield* shift of the C_{int} resonance, is consistent with the unsymmetrical coordination observed in the solid state. These ^{13}C NMR chemical shift data further imply that the coordinated olefin is polarized with a partial positive charge at C_{int} due to the coordination.[58] Consistent with this proposal, the H_{int} ^{1}H NMR resonance in **12a**,**b** and **20a**,**b** is shifted ca. 1.5 ppm downfield from the corresponding free olefin resonance, while the H_{cis} and H_{trans} resonances are much less affected by the coordination.

The X-ray structural and NMR data for **12a**,**b** and **20a**,**b** thus imply that in these species the Zr^+ center interacts primarily with C_{term} and polarizes the C=C double bond such that partial positive charge buildup occurs at C_{int}. The Zr−C interaction may be primarily electrostatic or, as illustrated by **C** in Chart 2, may involve overlap of one end of the C=C π-bonding orbital (i.e., the C_{term} p orbital) with the Zr σ-acceptor orbital. Alternatively, the Zr−olefin interaction may be represented in terms of resonance structures **D** (major) and **E** (minor) in Chart 2.

As noted in the Introduction, several other simple and chelated olefin complexes of d^0 metals have been characterized spectroscopically (Chart 1). The ^{13}C NMR data for the coordinated

(54) The activation parameters for olefin dissociation of **20a** ($\Delta H^{\ddagger}_{diss}$ and $\Delta S^{\ddagger}_{diss}$) were determined by averaging the activation parameters obtained from the simulations of the Me_{syn} resonances (Figure 7) and the C_5-indenyl H_α and H_β resonances (Figure 9). Because only half of the olefin dissociation events result in olefin face exchange, $k_{diss} = 2k_{FE}$ and $\Delta S^{\ddagger}_{diss} = \Delta S^{\ddagger}_{FE} + R\ln(2)$.

(55) Marsella, J. A.; Moloy, K. G.; Caulton, K. G. *J. Organomet. Chem.* **1980**, *201*, 389.

(56) (a) Emri, J.; Györi, B. In *Comprehensive Coordination Chemistry*; Wilkinson, G., Gillard, R. D., McCleverty, J. A., Eds.; Pergamon: Oxford, 1987; Vol. 3, p 82. (b) Lappert, M. F. *Chem. Rev.* **1956**, *56*, 959. (c) Steinberg, H.; Brotherton, R. J. *Organoboron Chemistry*; Wiley: New York, 1964; Vol. 1.

(57) (a) Jordan, R. F.; Bradley, P. K.; Baenziger, N. C.; LaPointe, R. E. *J. Am. Chem. Soc.* **1990**, *112*, 1289. (b) Alelyunas, Y. W.; Baenziger, N. C.; Bradley, P. K.; Jordan, R. F. *Organometallics* **1994**, *13*, 148.

(58) For discussions of the influence of charge and other factors on ^{13}C NMR shifts see: (a) Breitmaier, E.; Voelter, W. *Carbon-13 NMR Spectroscopy, High-Resolution Methods and Applications in Organic Chemistry and Biochemistry*, 3rd ed.; VCH: Weinheim, 1987; Chapter 3. (b) Mann, B. E.; Taylor, B. F. *^{13}C NMR Data for Organometallic Compounds*; Academic Press: London, 1981; pp 6−17.

Chart 2

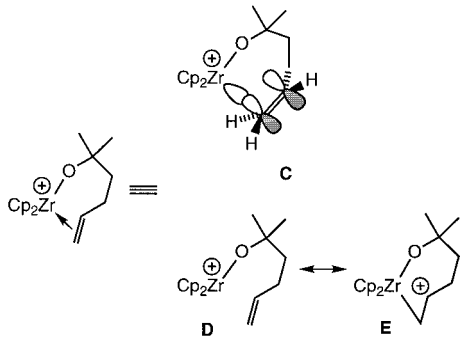

Chart 3

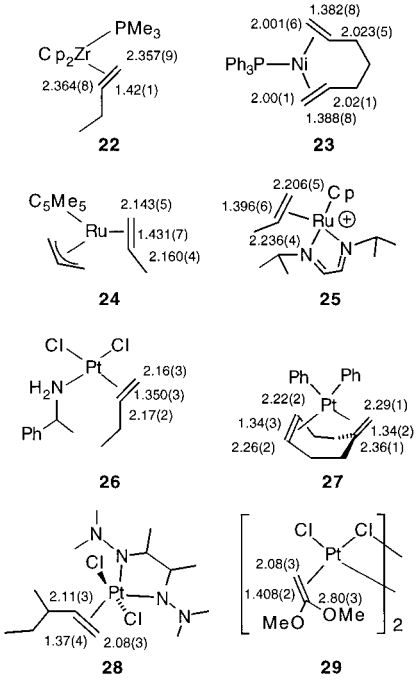

olefin units of the chelated species **3**−**6** are similar to the data for **12a**,**b** and **20a**,**b**. For example, the C_{int} and C_{term} resonances of **4** shift +36.2 and −22.7 ppm from the free olefin resonances, and the C_{int} and C_{term} resonances of **3** shift +15.0 and −1.0 ppm from the free olefin resonances. These NMR results imply that the olefin groups in **3**−**6** are also coordinated in an unsymmetrical fashion as established crystallographically for **12a** and **20a**. The C_{int} and C_{term} resonances for the V^V propene complex **2** are shifted +2.5 and −24 ppm from the free propene resonances, which is also consistent with unsymmetrical coordination and polarization of the olefin.

Comparison of d^0 and d^n ($n \geq 2$) Metal Olefin Complexes and Origin of Unsymmetrical Metal−Olefin Bonding. The results described above suggest that unsymmetrical metal−olefin coordination is a general feature of d^0 metal α-olefin complexes.[59] In contrast, conventional d^n ($n \geq 2$) metal α-olefin complexes normally exhibit symmetrical metal−olefin coordination, unless mitigating steric or electronic factors are present. Metal−olefin bond distances in several representative d^n ($n \geq 2$) metal complexes of unsymmetrical simple (i.e., no π-donor or -acceptor substituents) olefins are given in Chart 3. For **22**−**27**, the difference between the M−C_{term} and M−C_{int} bond distances (Δd_{M-C}) is less than 0.03 Å. The symmetrical coordination of butene to Zr^{II} in **22** is particularly significant because, as steric interactions are likely to be more severe in **22** than in **12a** due the shorter Zr−C distances in the former, it suggests that the unsymmetrical olefin coordination in **12a** is *not* due to olefin/Cp steric interactions.[33] Symmetrical propene and butene coordination is also observed in Ru^{II} and Pt^{II} species **24**−**26**.[60−62] Additionally, symmetrical olefin coordination is observed in the Ni^0 heptadiene complex **23**, despite incorporation of the olefin units in a chelate ring.[63] Less symmetrical olefin coordination is observed in crowded species, such as the five-coordinate 3-Me-1-pentene Pt^{II} complex **28** ($\Delta d_{M-C} = 0.03$ Å) and the 1,1-disubstituted olefin complex **27** ($\Delta d_{M-C} = 0.07$ Å), while very unsymmetrical coordination is observed when π-donor or -acceptor substituents are present on the olefin, e.g., **29**.[64−66] Therefore, the unsymmetrical olefin coordination observed in the solid-state structures of **12a** and **20a** ($\Delta d_{M-C} = 0.21$ and 0.18 Å, respectively) and implied by the NMR data for other d^0 olefin complexes probably reflects electronic rather than steric factors.

Chart 4

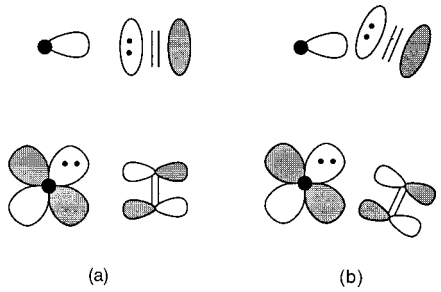

The symmetrical metal−olefin bonding in conventional d^n ($n \geq 2$) metal olefin complexes reflects the importance of d−π* back-bonding.[67] As illustrated in Chart 4, slippage of the olefin from a symmetrical (a) to an unsymmetrical (b) coordination mode reduces the d−π* overlap and weakens the metal−olefin bond. However, the σ-donation component of the metal−olefin bond is not strongly affected by olefin slippage, so unsymmetrical olefin bonding is not strongly disfavored for d^0 cases. Unsymmetrical coordination may be favored in cationic d^0 cases because the resulting polarization of the olefin π-bond provides a mechanism for delocalizing the metal charge.

Implications for $Cp_2M(R)(olefin)^+$ Bonding and Reactivity. The unsymmetrical metal−olefin bonding and resulting polarization of the olefin π-bonds in **12a**,**b**, **20a**,**b**, and **3**−**6** has important implications for the reactivity of alkyl olefin complexes of type **8**. Our results suggest that **8** is likely to adopt a similar unsymmetrical structure, especially when the olefin is an α-olefin.[59] Clearly, the resulting polarization of the olefin should enhance the nucleophilic migration of the alkyl ligand,

(59) The $(C_5R_5)_2Zr(OCMe_2CH_2CH_2CH{=}CH_2)^+$ species described here are models for $(C_5R_5)_2Zr(R)(CH_2{=}CHR)^+$ α-olefin adducts. More symmetrical olefin coordination may be expected for the corresponding ethylene complexes.

(60) Koelle, U.; Kang, B.-S.; Spaniol, T. P.; Englert, U. *Organometallics* **1992**, *11*, 249.
(61) de Klerk-Engels, B.; Delis, J. G. P.; Vrieze, K.; Goubitz, K.; Fraanje, J. *Organometallics* **1994**, *13*, 3269.
(62) Pedone, C.; Benedetti, E. *J. Organomet. Chem.* **1971**, *29*, 443.
(63) Proft, B.; Pörschke, K.-R.; Lutz, F.; Krüger, C. *Chem. Ber.* **1991**, *124*, 2667.
(64) Ammendola, P.; Ciajolo, M. R.; Panunzi, A.; Tuzi, A. *J. Organomet. Chem.* **1983**, *254*, 389.
(65) Rakowsky, M. H.; Woolcock, J. C.; Wright, L. L.; Green, D. B.; Rettig, M. F.; Wing, R. M. *Organometallics* **1987**, *6*, 1211.
(66) De Renzi, A.; Di Blasio, B.; Paiari, G.; Panunzi, A.; Pedone, C. *Gazz. Chim. Ital.* **1976**, *106*, 765.
(67) Mingos, D. M. P. In *Comprehensive Organometallic Chemistry*, 1st ed.; Wilkinson, G., Stone, F. G. A., Abel, E. W., Eds.; Pergamon: Oxford, UK, 1982; Vol 3, p 1.

i.e., should promote insertion. It has been appreciated for some time that the poor metal−olefin back-bonding and the associated generation of partial positive charge on the coordinated olefin is an important requirement for facile olefin insertion in early metal olefin polymerization catalysts. Our results support this concept and further suggest that unsymmetrical coordination may enhance this effect.

Olefin Face Exchange in $(C_5R_5)_2Zr(OCMe_2CH_2CH_2CH{=}CH_2)^+$ Species. The dynamic NMR results for **20a**,**b** show that olefin face exchange occurs by a dissociative mechanism without significant participation of σ-complex intermediates or anion assistance. It is more difficult to assess the significance of solvent assistance in the olefin dissociation. However, the similar dynamic behavior of **20a** in CD_2Cl_2 and C_6D_5Cl argues against significant solvent participation in the face exchange process of this species.

The olefin face exchange barrier for **20a**,**b** is significantly higher than that for **12a**,**b**. One possible reason for this difference is that the Zr−olefin bonding is stronger in **20a**,**b** than in **12a**,**b**. Structural and reactivity trends suggest that the *rac*-(EBI)Zr unit is more electron deficient than the Cp_2Zr unit. For example, the Zr−Cl distances in *rac*-(EBI)$ZrCl_2$ (2.3884(5) Å) are ca. 0.05 Å shorter than those in Cp_2ZrCl_2 (av 2.441(2) Å).[68,69] Additionally, Brintzinger et al. have reported that the apparent equilibrium constants for Me/Cl exchange between $(C_5R_5)_2ZrCl_2$ compounds and Al_2Me_6 in C_6D_6 (K_{obs} = [$(C_5R_5)_2$ZrMeCl][Al_2Me_5Cl]/[$(C_5R_5)_2ZrCl_2$][Al_2Me_6]) vary in the order *rac*-(EBI)$ZrCl_2$ (1.0(2) > Cp_2ZrCl_2 (0.49(4) > $(C_5H_2Me_3)_2ZrCl_2$ (0.0059(7)), which suggests that the Zr center in *rac*-(EBI)$ZrCl_2$ is more electron deficient than that in Cp_2ZrCl_2.[70] On the other hand, Mach et al. have found that the Zr $3d_{5/2}$ XPS core binding energies for *rac*-(EBI)$ZrCl_2$ and Cp_2ZrCl_2 are identical within experimental error (181.75(5) eV).[71] Thus, while differences in the Lewis acidity of *rac*-(EBI)$Zr(OR)^+$ and $Cp_2Zr(OR)^+$ may contribute to the difference in face exchange barriers, other factors may also be involved. In particular, it is possible that the face exchange barrier for **12a**,**b** is lowered by solvent participation, which is more important for **12a**,**b** than for **20a**,**b** because of the more sterically open structure of the former species. The activation entropy for face exchange of **12a** (−5(2) eu) is lower than that of **20a**,**b** (3(2) eu), which is consistent with increased solvent participation for **12a**. Alternatively, it is possible that steric interactions between the alkoxide linker and the EBI ligand increase the olefin dissociation barrier in **20a**,**b**. It may be possible to address these issues through studies of nonchelated systems. Finally, it should be noted that the face exchange barrier for {η^5:η^1-$C_5H_4SiMe_2N^tBu$}Ti{$OCMe_2CH_2CH_2CH{=}CH_2$}$^+$ (**30**; $\Delta H^{\ddagger}_{FE}$ = 12.2(9) kcal/mol; $\Delta S^{\ddagger}_{FE}$ = −2(3) eu) is much lower than that of {η^5:η^1-$C_5Me_4SiMe_2N^tBu$}Ti{$OCMe_2CH_2CH_2CH{=}CH_2$}$^+$ (**31**; $\Delta H^{\ddagger}_{FE}$ = 17.2(8) kcal/mol; $\Delta S^{\ddagger}_{FE}$ = 8(2) eu), despite the fact that the metal center in **30** is clearly more Lewis acidic than that in **31** due to differences in the cyclopentadienyl substituents.[20] Differences in the extent of solvent participation or cyclopentadienyl/alkoxide steric interactions may influence the face exchange barriers in this system as well.

Comparison to Computational Studies. The structures, bonding, and reactivity of Ti and Zr $(C_5R_5)_2MR^+$ and $(C_5R_5)_2MR(CH_2{=}CH_2)^+$ complexes have been investigated extensively at several levels of theory.[72] The results of these studies are consistent with the experimental results for the model systems reported here. Computational studies predict that $(C_5R_5)_2MR^+$ cations coordinate ethylene rather weakly (ΔH_{diss} < 20 kcal/mol) with little change in the structure of the olefin unit, and that $(C_5R_5)_2MR(CH_2{=}CH_2)^+$ species undergo insertion with low barriers (<10 kcal/mol). Most studies predict unsymmetrical metal olefin coordination in these systems with concomitant polarization of the C=C bond, and it is clear that the potential energy surface for rotation around the M−(olefin centroid) bond and perturbation of the $M-C_{olefin}$ distances is rather flat, as expected for weak M−olefin binding. For example, DFT calculations predict that the Zr−ethylene binding energy in $Cp_2Zr(CH_3)(CH_2{=}CH_2)^+$ is ca. 23 kcal/mol and that the Zr−ethylene coordination is unsymmetrical ($Zr-C_{central}$ = 2.72 Å; $Zr-C_{lateral}$ = 2.50 Å). The Zr−olefin bonding in $Cp_2Zr(Et)(CH_2{=}CH_2)^+$ is predicted to be weaker and more symmetrical.[72a,b]

Conclusions

A simple strategy has been developed for the synthesis of d^0 metal olefin complexes that is based on the use of the chelating alkoxide−olefin ligand $-OCMe_2CH_2CH_2CH{=}CH_2$. The metallocene complexes $Cp_2Zr(OCMe_2CH_2CH_2CH{=}CH_2)^+$ (in **12a**,**b**) and *rac*-(EBI)$Zr(OCMe_2CH_2CH_2CH{=}CH_2)^+$ (in **20a**,**b**), which are models for the corresponding $(C_5R_5)_2Zr(R)(\alpha\text{-olefin})^+$ species, adopt chelated structures in the solid state and in chlorocarbon solution. The Zr−olefin bonding in **12a**,**b** and **20a**,**b** is unsymmetrical and consists of a weak $Zr-C_{term}$ interaction and a minimal $Zr-C_{int}$ interaction. The Zr−olefin interaction does not perturb the structure of the coordinated olefin unit but does polarize the C=C bond such that positive charge buildup occurs at C_{int}. Similar unsymmetrical bonding and polarization effects may contribute to the high insertion reactivity of $(C_5R_5)_2Zr(R)(olefin)^+$ species. Dynamic NMR studies show that **12a**,**b** and **20a**,**b** undergo olefin face exchange in solution. The free energy barrier for face exchange for **20a** ($\Delta G^{\ddagger}_{FE}$ = 15.4(4) kcal/mol at 43 °C) is significantly greater than that for **12a** ($\Delta G^{\ddagger}_{FE}$ = 10.7(5) kcal/mol at −55 °C). The face exchange of **20a** is dissociative, with minimal involvement of anion, solvent, or σ-complex intermediates. The difference in face exchange barriers of **12a** and **20a** may reflect differences in Zr−olefin bond strengths, solvent participation in the olefin dissociation, or steric inhibition of chelate ring opening between the two cases. Studies of nonchelated analogues may help address these issues. The experimental results reported here are consistent with recent computational studies of $(C_5R_5)_2Zr(R)(olefin)^+$ species.

(68) Piemontesi, F.; Camurati, I.; Resconi, L.; Balboni, D. *Organometallics* **1995**, *14*, 1256.

(69) Prout, K.; Cameron, T. S.: Forder, R. A.; Critchley, S. R.; Denton, B.; Rees, G. V. *Acta Crystallogr.* **1974**, *B30*, 2290.

(70) (a) Beck, S.; Brintzinger, H. H. *Inorg. Chim. Acta* **1998**, *270*, 376. See also: (b) Finch, W. C.; Anslyn, E. V.; Grubbs, R. H. *J. Am. Chem. Soc.* **1988**, *110*, 2406.

(71) (a) Bastl, Z.; Mach, K. Private communication. Published values for the Zr $3d_{5/2}$ XPS core binding energy of Cp_2ZrCl_2 range from 181.7 to 182.0 eV. See: (b) Gassman, P. G.; Callstrom, M. R. *J. Am. Chem. Soc.* **1987**, *109*, 7875. (c) Gassman, P. G.; Macomber, D. W.; Hershberg, J. W. *Organometallics* **1983**, *2*, 1470. (d) Siedle, A. R.; Newmark, R. A.; Lamanna, W. M.; Schroepfer, J. N. *Polyhedron* **1990**, *9*, 301.

(72) Leading references: (a) Lohrenz, J. C. W.; Woo, T. K.; Fan, L.; Ziegler, T. *J. Organomet. Chem.* **1995**, *497*, 91. (b) Woo, J. K.; Fan, L.; Ziegler, T. *Organometallics* **1994**, *13*, 2252. (c) Lohrenz, J. C. W.; Woo, T. K.; Ziegler, T. *J. Am. Chem. Soc.* **1995**, *117*, 12793. (d) Weiss, H.; Ehrig, M.; Ahlrichs, R. *J. Am. Chem. Soc.* **1994**, *116*, 4919. (e) Meier, R. J.; van Doremaele, G. H. J.; Iarlori, S.; Buda, F. *J. Am. Chem. Soc.* **1994**, *116*, 7274. (f) Castonguay, L. A.; Rappé, A. K. *J. Am. Chem. Soc.* **1992**, *114*, 5832. (g) Yoshida, T.; Koga, N.; Morokuma, K. *Organometallics* **1996**, *15*, 766. (h) Yoshida, T.; Koga, N.; Morokuma, K. *Organometallics* **1995**, *14*, 746. (i) Prosenc, M. H.; Janiak, C.; Brintzinger, H. H. *Organometallics* **1992**, *11*, 4036. (j) Jolly, C.; Marynick, D. *J. Am. Chem. Soc.* **1989**, *111*, 7968. (k) Margl, P.; Deng, L.; Ziegler, T. *Organometallics* **1998**, *17*, 933. (l) Prosenc, M. H.; Brintzinger, H. H. *Organometallics* **1997**, *16*, 3889.

Experimental Section

General Procedures. All manipulations were performed using glovebox or Schlenk techniques under a purified N_2 atmosphere, or on a high-vacuum line. Solvents were distilled from appropriate drying/deoxygenating agents and stored under N_2 prior to use (toluene, hexane, Et_2O, and C_6D_6, Na/benzophenone; CD_2Cl_2 and C_6D_5Cl, P_2O_5; $CDCl_2$-$CDCl_2$ and $CHCl_2CHCl_2$, molecular sieves). Alcohols were purchased from Wiley Organics and dried with Na before use or prepared as described below. $B(C_6F_5)_3$ was provided by Boulder Scientific, and $[Ph_3C][B(C_6F_5)_4]$ was provided by Asahi Glass Co. Cp_2ZrMe_2[73] and *rac*-(EBI)$ZrMe_2$[74] were prepared by literature procedures. IR spectra were recorded on a Mattson Cygnus 25 instrument. Elemental analyses were performed by E+R Microanalytical Laboratory, Inc.

NMR spectra were recorded on a Bruker AMX-360 or DMX-500 spectrometer, in flame-sealed or Teflon-valved tubes, at 23 °C unless otherwise indicated. ^1H and ^{13}C chemical shifts are reported vs $SiMe_4$ and were determined by reference to the residual ^1H and ^{13}C solvent peaks. ^{11}B NMR are referenced to external $Et_2O{\cdot}BF_3$. ^{19}F NMR spectra were recorded on a Bruker AC-300 spectrometer, and chemical shifts are reported vs $CFCl_3$. All coupling constants are reported in hertz. C−H coupling constants were determined from gated-^1H-decoupled ^{13}C spectra. Variable-temperature NMR experiments were performed on an AMX-360 spectrometer equipped with a Brüker B-VT-1000E variable-temperature unit with a Eurotherm 818 controller. The temperature controller was calibrated by measuring the chemical shift difference between the methyl and OH resonances of a 4% solution of MeOH in CD_3OD between −93 and 27 °C and fitting these data to a calibration curve provided by Bruker.[75] Homonuclear gradient-selected phase-sensitive multiple-quantum-filtered COSY (cosygsmtp) spectra and phase-sensitive NOESY/EXSY (noesytp) spectra were acquired and processed according to literature procedures using standard Bruker programs.[76]

2-Methyl-5-hexen-2-ol. A solution of 5-hexen-2-one (10.0 g, 102 mmol) in Et_2O (60 mL) was cooled to −78 °C, and MeMgBr (3 M in Et_2O, 40.0 mL, 120 mmol) was added via cannula, yielding a cloudy white solution. The mixture was allowed to warm to 23 °C, stirred for 18 h, and quenched with water (50 mL). The two phases were separated, and the aqueous layer was extracted with Et_2O (3 × 30 mL). The organic phase and the ether extracts were combined, extracted with water (3 × 30 mL), and dried over Na_2SO_4. The solvent was removed under vacuum. The crude product was distilled at 28−31 °C under reduced pressure, yielding a colorless liquid (7.5 g, 64%). ^1H NMR (CD_2Cl_2): δ 5.86 (m, 1H, vinyl H_{int}), 5.04 (dq, J = 17.1 and 2.0, 1H, vinyl H_{trans}), 4.94 (dm, J = 10.0, 1H, vinyl H_{cis}), 2.13 (m, 2H, CH_2), 1.54 (m, 2H, CH_2), 1.27 (s, 1H, OH), 1.19 (s, 6H, CH_3). ^{13}C NMR (CD_2Cl_2): δ 139.7 (d, J_{C-H} = 151, *C*H═), 114.3 (t, J_{C-H} = 156, ═*C*H_2), 70.9 (O*C*), 43.3 (*C*H_2), 29.5 (*C*H_3), 29.2 (*C*H_2).

2-Methyl-6-hepten-2-ol. A degassed solution of 5-bromopentene (5.00 g, 32.5 mmol) in Et_2O (20 mL) was added to a mixture of Mg turnings (1.20 g, 49.4 mmol) and dry Et_2O (40 mL) under N_2 at 23 °C via cannula over a period of 1 h. The mixture was stirred at 23 °C for 2 h. The liquid phase was transferred via cannula from the excess Mg, and added dropwise via cannula to a solution of acetone (3.0 mL, 41 mmol) in Et_2O (20 mL). A white precipitate formed immediately. The reaction mixture was quenched with aqueous $[NH_4]Cl$ and filtered. The filtrate was washed with H_2O and the solvent removed under vacuum, yielding a colorless oil. The oil was purified by column chromatography on silica gel; elution with ethyl acetate/petroleum ether (3:20) provided 1.2 g (29%) of pure 2-methyl-6-hepten-2-ol. ^1H NMR ($CDCl_3$): δ 5.79 (m, 1H, vinyl H_{int}), 4.99 (dq, J = 17.1 and 2, 1H, vinyl H_{trans}), 4.94 (dq, J = 9.1 and 2, 1H, vinyl H_{cis}), 2.04 (m, 2H, CH_2), 1.45 (m, 4H, CH_2), 1.36 (s, 1H, O*H*), 1.19 (s, 6H, CH_3). ^{13}C NMR (CD_2Cl_2): δ 139.4 (═*C*H), 114.5 (═*C*H_2), 70.9 (O*C*), 43.8 (*C*H_2), 34.6 (*C*H_2), 29.4 (*C*H_3), 24.1 (*C*H_2). EI−HRMS: *m*/*z* calcd for $C_8H_{16}O$ ($M^+ - CH_3$), 113.0966; found 113.0963.

$[NBu_3(CH_2Ph)][MeB(C_6F_5)_3]$. A solution of $B(C_6F_5)_3$ (1.02 g, 2.0 mmol) in Et_2O (125 mL) was cooled to −78 °C, and MeLi (1.6 mL, 1.4 M in Et_2O, 2.2 mmol) was added dropwise over 5 min. The solution was allowed to warm to 23 °C over 18 h. The solvent was removed under vacuum, yielding a white solid ($Li[MeB(C_6F_5)_3]$). The white solid was dissolved in degassed water (40 mL), and a solution of $[NBu_3(CH_2Ph)]Cl$ (0.75 g, 2.4 mmol) in degassed water (10 mL) was added. The resulting white suspension was stirred for 18 h. The mixture was extracted with Et_2O (3 × 40 mL), and the extracts were dried over $MgSO_4$. The solvent was removed from the extract under vacuum, yielding a white solid. The solid was dissolved in toluene and dried over molecular sieves (4 Å) for 5 d. The solution was decanted, and the solvent was removed under vacuum, yielding an off-white solid (860 mg, 54%). ^1H NMR (C_6D_5Cl): δ 7.23 (m, 3H), 6.92 (d, J = 6.8, 2H), 3.67 (s, 2H), 2.45 (m, 6H), 1.29 (m, 6H), 1.11 (br s, 3H, MeB, partially obscured), 1.06 (sex, J = 7.2, 6H), 0.79 (t, J = 7.3, 9H). ^1H NMR (CD_2Cl_2): δ 7.55 (m, 3H), 7.31 (d, J = 8, 2H), 4.25 (s, 2H), 3.00 (m, 6H), 1.74 (m, 6H), 1.40 (m, 6H), 1.02 (t, J = 7.3, 9H), 0.47 (br s, 3H, MeB). $^{13}C\{^1H\}$ NMR (CD_2Cl_2): δ 148.7, (d, J_{C-F} = 242, anion), 137.8 (d, J_{C-F} = 243, anion), 136.8 (d, J_{C-F} = 242, anion), 132.1 (2C), 130.3, 125.7, 62.8, 59.6, 24.3, 19.8, 10.0 (br, BMe), 13.5, 1.1, anion quarternary carbon not observed. ^{19}F NMR (CD_2Cl_2): δ −133.1 (d, J_{F-F} = 20, 2F), −165.0 (t, J_{F-F} = 20, 1F), −167.8 (m, 2F). Anal. Calcd for $C_{38}H_{37}BF_{15}N$: C, 56.80; H, 4.64. Found: C, 56.55; H, 4.52.

$Cp_2Zr(OCMe_2CH_2CH_2CH{=}CH_2)Me$ (9). Neat 2-methyl-5-hexen-2-ol (0.144 mL, 1.09 mmol) was added dropwise to a solution of Cp_2ZrMe_2 (0.249 g, 0.99 mmol) in CH_2Cl_2 (8.0 mL) at 23 °C. The mixture was stirred at 23 °C for 5 min, and the volatiles were removed under vacuum, yielding **9** as a colorless oil (100%). ^1H NMR (CD_2Cl_2): δ 6.00 (s, 10H, C_5H_5), 5.86 (m, 1H, vinyl H_{int}), 5.04 (dq, J = 17.1 and 2, 1H, vinyl H_{trans}), 4.94 (dq, J = 10.1 and 2, 1H, vinyl H_{cis}), 2.01 (m, 2H, CH_2), 1.40 (m, 2H, CH_2), 1.08 (s, 6H, CH_3), −0.002 (s, 3H, ZrCH_3). ^{13}C NMR (CD_2Cl_2): δ 140.0 (d, J_{C-H} = 151, ═*C*H), 113.9 (t, J_{C-H} = 154, ═*C*H_2), 110.4 (d, J_{C-H} = 171,*C*$_5H_5$), 79.3 (O*C*), 43.9 (t, J_{C-H} = 124, *C*H_2), 30.6 (t, J_{C-H} = 125, *C*H_2), 29.2 (q, J_{C-H} = 125, *C*H_3), 17.4 (q, J_{C-H} = 119, Zr*C*H_3). Anal. Calcd for $C_{18}H_{26}OZr$: C, 61.84; H, 7.50. Found: C, 61.85; H, 7.54.

Generation of $Cp_2Zr(OCMe_2CH_2CH{=}CH_2)Me$ (10). A solution of Cp_2ZrMe_2 (15.2 mg, 0.060 mmol) in CD_2Cl_2 (0.5 mL) was prepared in a Teflon-valved NMR tube, and $HOCMe_2CH_2CH{=}CH_2$ (7.4 μL, 0.060 mmol) was added via a microsyringe. The tube was sealed and vigorously agitated, and NMR spectra were recorded. The conversion to **10** was quantitative. ^1H NMR (CD_2Cl_2): δ 6.00 (s, 10H, C_5H_5), 5.78 (m, 1H, vinyl H_{int}), 5.02 (m, 2H, ═CH_2), 2.08 (d, J = 7.2, 2H, CH_2), 1.06 (s, 6H, CH_3), −0.01 (s, 3H, ZrCH_3). ^{13}C NMR (CD_2Cl_2): δ 136.3 (═*C*H), 116.7 (═*C*H_2), 110.5 (*C*$_5H_5$), 79.3 (O*C*), 49.4 (*C*H_2), 29.8 (*C*H_3), 17.4 (Zr*C*H_3).

Generation of $Cp_2Zr(OCMe_2(CH_2)_3CH{=}CH_2)Me$ (11). Compound **11** was generated quantitatively by the reaction of Cp_2ZrMe_2 (11.3 mg, 0.045 mmol) and $HOCMe_2(CH_2)_3CH{=}CH_2$ (7.0 μL, 0.046 mmol), using the procedure described above for **10**. ^1H NMR (CD_2Cl_2): δ 5.99 (s, 10H, C_5H_5), 5.86 (m, 1H, vinyl H_{int}), 4.99 (m, 2H, ═CH_2), 2.03 (m, 2H, CH_2), 1.33 (m, 4H, CH_2), 1.05 (s, 6H, CH_3), −0.03 (s, 3H, ZrCH_3). ^{13}C NMR (CD_2Cl_2): δ 139.7 (═*C*H), 114.3 (═*C*H_2), 110.4 (*C*$_5H_5$), 79.6 (O*C*), 44.3 (*C*H_2), 34.7 (*C*H_2), 29.9 (*C*H_3), 24.1 (*C*H_2), 17.2 (Zr*C*H_3).

$[Cp_2Zr(OCMe_2CH_2CH_2CH{=}CH_2)][MeB(C_6F_5)_3]$ (12a). A solution of $B(C_6F_5)_3$ (0.507 g, 0.99 mmol) in CH_2Cl_2 (5 mL) was added to a solution of **9** (0.346 g, 0.99 mmol) in CH_2Cl_2 (4 mL). The resulting yellow solution was stirred at 23 °C for 10 min. The solvent was removed under vacuum, and the residue was recrystallized from CH_2Cl_2/pentane, yielding **12a** as a pale yellow powder, which was dried under vacuum (0.804 g, 94.3%). ^1H NMR (CD_2Cl_2, −80 °C): δ 7.50

(73) Samuel, E.; Rausch, M. D. *J. Am. Chem. Soc*. **1973**, *95*, 6263.
(74) (a) Diamond, G. M.; Jordan, R. F.; Petersen, J. L. *J. Am. Chem. Soc.* **1996**, *118*, 8024. (b) Diamond, G. M.; Rodewald, S.; Jordan, R. F. *Organometallics* **1995**, *14*, 5.
(75) (a) Bruker B-VT-1000E variable-temperature unit manual, page 13. (b) Van Geet, A. L. *Anal. Chem.* **1970**, *42*, 679.
(76) (a) Hurd, R. E. *J. Magn. Reson.* **1990**, *87*, 422. (b) Bereton, I. M.; Crozier, S.; Field, J.; Doddrell, D. M. *J. Magn. Reson.* **1991**, *93*, 54. (c) Davis. A. L.; Laue, E. D.; Keeler, J.; Moskau, D.; Lohman, J. *J. Magn. Reson.* **1991**, *94*, 637. (d) Jeener, J.; Meier, B. H.; Bachman, P.; Ernst, R. R. *J. Chem. Phys.* **1979**, *71*, 4546. (e) Perrin, C. L.; Gipe, *J. Am. Chem. Soc.* **1984**, *106*, 4036. (f) Batta, G.; Banyai, I.; Glaser, J. *J. Am. Chem. Soc.* **1993**, *115*, 6782.

(m, 1H, vinyl H_{int}), 6.42 (s, 5H, C_5H_5), 6.39 (s, 5H, C_5H_5), 5.35 (d, J = 20.5, 1H, vinyl H_{trans}), 4.58 (d, J = 8.6, 1H, vinyl H_{cis}), 2.48 (br, 1H, CH_2), 2.02 (br, 2H, CH_2), 1.17 (s, 3H, CH_3), 1.08 (s, 3H, CH_3), 0.39 (s, 3H, BCH_3). ^{1}H NMR (CD_2Cl_2, 23 °C): δ 7.51 (br m, 1H, vinyl H_{int}), 6.46 (s, 10H, C_5H_5), 5.40 (br d, J = 17.9, 1H, vinyl H_{trans}), 4.62 (d, J = 8.8, 1H, vinyl H_{cis}), 2.31 (br m, 2H, CH_2), 2.08 (br m, 2H, CH_2), 1.25 (s, 6H, CH_3), 0.50 (br s, 3H, BCH_3). ^{13}C NMR (CD_2Cl_2, −80 °C): δ 158.8 (d, J_{C-H} = 151, =*C*H), 114.6 (d, J_{C-H} = 169, C_5H_5), 114.2 (d, J_{C-H} = 169, C_5H_5), 94.3 (t, J_{C-H} = 157, =*C*H_2), 83.6 (s, O*C*), 48.6 (t, J_{C-H} = 130, *C*H_2), 31.1 (t, J_{C-H} = 130, *C*H_2), 29.1 (q, J_{C-H} = 125, *C*H_3), 25.2 (q, J_{C-H} = 125, *C*H_3), 9.2 (B*C*H_3). ^{13}C NMR (CD_2Cl_2, 23 °C): δ 159.2 (d, J_{C-H} = 150, =*C*H), 115.5 (d, J_{C-H} = 175, C_5H_5), 95.9 (t, J_{C-H} = 160, =*C*H_2), 84.9 (s, O*C*), 49.1 (t, J_{C-H} = 126, *C*H_2), 31.9 (t, J_{C-H} = 133, *C*H_2), 28.3 (q, J_{C-H} = 126, *C*H_3), 10.1 (B*C*H_3). ^{19}F NMR (CD_2Cl_2): δ −133.0 (d, J_{F-F} = 21, 2F), −164.9 (t, J_{F-F} = 20, 1F), −167.6 (t, J_{F-F} = 22, 2F). Anal. Calcd for $C_{36}H_{26}F_{15}$BOZr: C, 50.18; H, 3.04. Found: C, 49.97; H, 3.33.

Generation of [$Cp_2Zr(OCMe_2CH_2CH_2CH{=}CH_2)$][$B(C_6F_5)_4$] (12b). Solid [$Ph_3C$][$B(C_6F_5)_4$] (51 mg, 0.055 mmol) was added to a solution of **9** (19 mg, 0.055 mmol) in C_6D_6 (ca. 2 mL) at 23 °C in an NMR tube. Almost instantaneously, gas evolution was observed and an orange oil appeared, while the upper benzene layer remained colorless. The tube was vigorously shaken and allowed to stand at room temperature for 1 h. The volatiles were removed under vacuum, affording an orange powder, and CD_2Cl_2 was added by vacuum transfer. The ^{1}H NMR spectrum of the resulting orange solution established that **12b** had formed quantitatively. The ^{1}H NMR resonances for the $Cp_2Zr(OCMe_2CH_2CH_2CH{=}CH_2)^+$ cation are identical to those for the corresponding $MeB(C_6F_5)_3^-$ salt **12a**. Resonances for Ph_3CMe were also observed.

Generation of [$Cp_2Zr(OCMe_2CH_2CH_2CH{=}CH_2)$(THF)][$MeB(C_6F_5)_3$] (13). A solution of **12a** (25 mg, 0.029 mmol) in CD_2Cl_2 (0.5 mL) was prepared in a Teflon-valved NMR tube, and THF (7.2 μL, 0.087 mmol) was added via a microsyringe. The tube was sealed and vigorously agitated, the volatiles were removed under vacuum, and CD_2Cl_2 was added. NMR spectra were recorded and showed that **13** had formed quantitatively. ^{1}H NMR (CD_2Cl_2): δ 6.47 (s, 10H, C_5H_5), 5.84 (m, 1H, vinyl H_{int}), 5.07 (d, J = 17.1, 1H, vinyl H_{trans}), 5.00 (d, J = 10.2, 1H, vinyl H_{cis}), 4.04 (m, 4H, THF), 2.17 (m, 4H, THF), 2.04 (m, 2H, CH_2), 1.61 (m, 2H, CH_2), 1.27 (s, 6H, CH_3), 0.508 (br s, 3H, BCH_3). ^{13}C NMR (CD_2Cl_2): δ 138.1 (d, J_{C-H} = 152, =*C*H), 115.5 (d, J_{C-H} = 175, C_5H_5), 115.1 (t, J_{C-H} = 156, =*C*H_2), 86.2 (s, O*C*), 79.0 (t, J = 150, THF), 43.9 (t, J_{C-H} = 126, *C*H_2), 29.7 (q, J_{C-H} = 125, *C*H_3), 29.6 (t, J_{C-H} = 126, *C*H_2), 26.1 (t, J_{C-H} = 132, THF), 9.9 (br, B*C*H_3). ^{19}F NMR (CD_2Cl_2): δ −133.0 (d, J_{F-F} = 21, 2F), −165.1 (t, J_{F-F} = 20, 1F), −167.7 (t, J_{F-F} = 22, 2F).

Generation of [$Cp_2Zr(OCMe_2CH_2CH_2CH{=}CH_2)(Et_2O)$][$MeB(C_6F_5)_3$] (14). A solution of **12a** (10.2 mg, 0.012 mmol) in CD_2Cl_2 (0.5 mL) was prepared in a Teflon-valved NMR tube, and Et_2O (3.7 μL, 0.035 mmol) was added via a microsyringe. The tube was sealed and vigorously agitated, the volatiles were removed under vacuum, and CD_2Cl_2 was added. NMR spectra were recorded and showed that **14** had formed quantitatively. ^{1}H NMR (CD_2Cl_2): δ 6.51 (s, 10H, C_5H_5), 5.84 (m, 1H, vinyl H_{int}), 5.08 (dq, J = 17.1 and 1.6, 1H, vinyl H_{trans}), 5.02 (dq, J = 10.2 and 1.5, 1H, vinyl H_{cis}), 3.97 (q, J = 7.1, 4H, CH_2), 2.04 (m, 2H, CH_2), 1.61 (m, 2H, CH_2), 1.43 (t, J = 7.1, 6H, CH_3), 1.28 (s, 6H, CH_3), 0.49 (br s, 3H, BCH_3). The ^{1}H NMR spectrum of **14** in the presence of excess Et_2O is unchanged except for the presence of free Et_2O resonances, indicating that only 1 equiv of Et_2O coordinates and exchange of free and coordinated Et_2O is slow.

Generation of [$Cp_2Zr(OCMe_2CH_2CH{=}CH_2)$][$MeB(C_6F_5)_3$] (15). A solution of **10** (0.060 mmol) in CD_2Cl_2 (0.5 mL) was prepared as described above. The volatiles were removed under vacuum, and a solution of $B(C_6F_5)_3$ (1.0 equiv) in CD_2Cl_2 (0.5 mL) was added. The tube was sealed and agitated at 23 °C, and NMR spectra were recorded. Complex **15** was formed quantitatively. ^{1}H NMR (CD_2Cl_2): δ 6.43 (s, 10H, C_5H_5), 5.68 (m, 1H, vinyl H_{int}), 5.07 (m, 2H, =CH_2), 2.13 (d, J = 7.2, 2H, CH_2), 1.15 (s, 6H, CH_3), 0.72 (br s, 3H, BCH_3). ^{13}C NMR (CD_2Cl_2): δ 133.6 (d, J_{C-H} = 151, =*C*H), 118.5 (t, J_{C-H} = 166, =*C*H_2), 114.9 (d, J_{C-H} = 179, C_5H_5), 86.0 (s, O*C*), 48.2 (t, J_{C-H} = 122, *C*H_2), 28.4 (q, J_{C-H} = 126, *C*H_3), 2.7 (br, B*C*H_3). ^{19}F NMR (CD_2Cl_2): δ −133.4 (d, J_{F-F} = 22, 2F), −164.4 (t, J_{F-F} = 20, 1F), −166.2 (t, J_{F-F} = 19, 2F).

Generation of [$Cp_2Zr(OCMe_2CH_2CH{=}CH_2)$(THF)][$MeB(C_6F_5)_3$] (16). Compound **16** was generated quantitatively from **15** using the procedure described above for **13**. ^{1}H NMR (CD_2Cl_2): δ 6.48 (s, 10H, C_5H_5), 5.78 (m 1H, vinyl H_{int}), 5.17 (m, 2H, =CH_2), 4.04 (br s, 4H, THF), 2.28 (d, J = 7.3, 2H, CH_2), 2.16 (br s, 4H, THF), 1.28 (s, 6H, CH_3), 0.51 (br s, 3H, BCH_3). ^{13}C NMR (CD_2Cl_2): δ 133.9 (d, J_{C-H} = 153, =*C*H), 119.2 (t, J_{C-H} = 156, =*C*H_2), 115.5 (d, J_{C-H} = 174, C_5H_5), 85.8 (s, O*C*), 79.0 (t, J_{C-H} = 153, THF), 49.1 (t, J_{C-H} = 123, *C*H_2), 29.8 (q, J_{C-H} = 126, *C*H_3), 26.1 (t, J_{C-H} = 135, THF), 10.3 (br, B*C*H_3). ^{19}F NMR (CD_2Cl_2): δ −133.0 (d, J_{F-F} = 21, 2F), −165.0 (t, J_{F-F} = 20, 1F), −167.6 (t, J_{F-F} = 21, 2F).

Generation of [$Cp_2Zr(OCMe_2(CH_2)_3CH{=}CH_2)$][$MeB(C_6F_5)_3$] (17/17′). Compound **11** was converted to **17**/**17′** using the procedure described above for the conversion of **10** to **15**. Compound **17**/**17′** was formed in 93% yield by ^{1}H NMR. Low-temperature NMR spectra show that this compound exists as a mixture of olefin adduct **17** and ion pair **17′** (ratio 1.2/1 at −90 °C). Spectra data for these species are listed separately. The resonances for **17** and **17′** are coalesced in the 23 °C spectrum.

Data for 17. ^{1}H NMR (CD_2Cl_2, −80 °C): δ 7.40 (m, 1H, vinyl H_{int}), 6.41 (s, 5H, C_5H_5), 6.40 (s, 5H, C_5H_5), 5.25 (d, J = 18.3, 1H, vinyl H_{trans}), 4.69 (d, J = 8.4, 1H, vinyl H_{cis}), 2.89 (br m, 1H, CH_2), 2.20 (br m, 1H, CH_2), 1.5−1.8 (br m, 4H, CH_2), 1.27 (s, 3H, CH_3), 1.15 (s, 3H, CH_3), 0.38 (br s, 3H, BCH_3). ^{13}C NMR (CD_2Cl_2, −80 °C): δ 157.9 (d, J_{C-H} = 157, =*C*H), 114.3 (*C*$_5$H$_5$), 114.0 (*C*$_5$H$_5$), 92.6 (=*C*H_2), 87.9 (O*C*), 42.3 (*C*H_2), 36.9 (*C*H_2), 32.0 (*C*H_3), 26.2 (*C*H_3), 20.3 (CH_2), 9.1 (B*C*H_3).

Data for 17′. ^{1}H NMR (CD_2Cl_2, −80 °C): δ 6.35 (s, 10H, C_5H_5), 5.71 (m, 1H, vinyl H_{int}), 4.92 (m, 2H, =CH_2), 1.87 (br m, 2H CH_2,), 0.9−1.5 (br m, 4H, CH_2), 0.60 (br s, 3H, BCH_3). ^{13}C NMR (CD_2Cl_2, −80 °C): δ 138.2 (=*C*H), 114.5 (*C*$_5$H$_5$), 114.2 (*C*H_2), 85.2 (O*C*), 40.1 (*C*H_2), 33.6 (*C*H_2), 28.1 (*C*H_3), 23.4 (*C*H_2), 1.9 (B*C*H_3). ^{19}F NMR (CD_2Cl_2): δ −133.3 (d, J_{F-F} = 22, 2F), −162.6 (t, J_{F-F} = 20, 1F), −166.3 (t, J_{F-F} = 21, 2F).

Generation of [$Cp_2Zr(OCMe_2(CH_2)_3CH{=}CH_2)$(THF)][$MeB(C_6F_5)_3$] (18). Compound **18** was generated from **17**/**17′** by the procedure described above for **13**. The conversion was quantitative. ^{1}H NMR (CD_2Cl_2): δ 6.46 (s, 10H, C_5H_5), 5.84 (m, 1H, vinyl H_{int}), 5.01 (m, 2H, =CH_2), 4.03 (m, 4H, THF), 2.16 (m, 4H, THF), 2.11 (q, J = 7.3, 2H, CH_2), 1.51 (m, 2H, CH_2), 1.49 (m, 2H, CH_2), 1.25 (s, 6H, CH_3), 0.51 (s, 3H, BCH_3). ^{13}C NMR (CD_2Cl_2): δ 140.0 (d, J_{C-H} = 148, =*C*H), 116.7 (d, J_{C-H} = 180, C_5H_5), 115.2 (t, J_{C-H} = 155, =*C*H_2), 86.5 (s, O*C*), 78.9 (t, J_{C-H} = 153, *C*H_2), 44.3 (t, J_{C-H} = 131, *C*H_2), 34.2 (t, J_{C-H} = 122, *C*H_2), 29.6 (q, J_{C-H} = 126, *C*H_3), 26.1 (t, J_{C-H} = 135, *C*H_2), 25.7 (t, J_{C-H} = 133, *C*H_2), 10.3 (br, B*C*H_3). ^{19}F NMR (CD_2Cl_2): δ −133.0 (d, J_{F-F} = 21, 2F), −165.0 (t, J_{F-F} = 20, 1F), −166.6 (t, J_{F-F} = 20, 2F).

***rac*-(EBI)Zr(OCMe$_2$CH$_2$CH$_2$CH=CH$_2$)(Me) (19)**. A flask was charged with *rac*-(EBI)$ZrMe_2$ (0.19 g, 0.50 mmol), 2-methyl-5-hexen-2-ol (0.066 g, 0.57 mmol), and C_6H_6 (20 mL). The solution was stirred for 18 h at 23 °C, and the volatiles were removed under reduced pressure, yielding *rac*-(EBI)Zr(OCMe$_2$CH$_2$CH$_2$CH=CH$_2$)(Me) (**19**) as yellow oily crystals. ^{1}H NMR (CD_2Cl_2): δ 7.75 (d, J = 8.8, 1H, indenyl), 7.44 (d, J = 8.8, 1H, indenyl), 7.33 (d, J = 8.8, 1H, indenyl), 7.23 (d, J = 8.8, 1H, indenyl), 7.15−7.00 (m, 4H, indenyl), 6.36 (d, J = 3.2, 1H, C_5-indenyl), 6.31 (d, J = 2.9, 1H, C_5-indenyl), 6.00 (d, J = 3.2, 1H, C_5-indenyl), 5.84 (d, J = 3.1, 1H, C_5-indenyl), 5.88−5.77 (m, 1H, vinyl H_{int}), 5.01 (d, J = 17.2, 1H, vinyl H_{trans}), 4.95 (d, J = 9.6, 1H, vinyl H_{cis}), 3.62−3.27 (m, 4H, −CH_2CH_2− bridge), 1.78 (m, 2H, CH_2), 1.17 (m, 2H, CH_2), 0.83 (s, 3H, Me), 0.81 (s, 3H, Me), −1.08 (s, 3H, ZrMe). ^{13}C NMR (CD_2Cl_2): δ 140.1 (d, J_{C-H} = 150, CH=), 127.4 (C), 125.6 (C), 125.3 (CH), 124.4 (CH), 123.8 (CH), 123.7 (CH), 123.7 (CH), 123.3 (CH), 123.0 (C), 122.5 (CH), 121.6 (C), 120.8 (CH), 118.5 (C), 115.3 (C), 114.3 (CH), 113.7 (t, J_{C-H} = 155, =CH_2), 109.4 (CH), 103.4 (CH), 100.0 (CH), 80.6 (C), 43.8 (CH_2), 30.1 (CH_3), 30.0 (CH_3), 28.9 (CH_2), 27.9 (CH_2), 27.6 (CH_2), 25.8 (CH_3).

[*rac*-(EBI)Zr(OCMe$_2$CH$_2$CH$_2$CH=CH$_2$)][MeB(C$_6$F$_5$)$_3$] (20a). The *rac*-(EBI)Zr(OCMe$_2$CH$_2$CH$_2$CH=CH$_2$)(Me) (**19**) from above was dissolved in toluene (15 mL). A solution of $B(C_6F_5)_3$ (0.26 g, 0.50 mmol)

in toluene (15 mL) was added dropwise, resulting in the immediate formation of an orange oil. The toluene was decanted away, and the oil was dried under reduced pressure for 18 h. The oil was dissolved in $CHCl_2CHCl_2$ (10 mL), and the solution was layered with pentane (15 mL). After 2 d at −20 °C, red crystals of [*S,S,R/R,R,S*-(EBI)Zr(OCMe$_2$CH$_2$CH$_2$CH=CH$_2$)] [MeB(C$_6$F$_5$)$_3$]·$CHCl_2CHCl_2$ (**20a**·$CHCl_2CHCl_2$) were isolated (0.30 g, 52% based on a 1/1 isomer ratio in solution). In CD_2Cl_2, $CDCl_2CDCl_2$, or C_6D_5Cl solution, **20a** exists as a 1/1 mixture of two diastereomers which undergo exchange as described in the text. ^{1}H NMR (C_6D_5Cl, −35 °C, slow isomer exchange): δ 7.52 (d, J = 8.2, 1H, indenyl), 7.39−6.84 (m, indenyl and vinyl H$_{int}$ of *S,S,R*; partially obscured by solvent), 6.44 (m, 1H, vinyl H$_{int}$ of *S,S,S*), 5.99 (d, J = 3.3, 1H, C$_5$-α1 or α3), 5.81 (d, J = 3.2, 1H, C$_5$-*β*2), 5.77 (d, J = 3.0, 1H, C$_5$-*β*1 or *β*3), 5.76 (d, J = 3.0, 1H, C$_5$-*β*1 or *β*3), 5.67 (d, J = 3.3, 1H, C$_5$-α1 or α3), 5.66 (d, J = 3.2, 1H, C$_5$-α4), 5.64 (d, J = 3.2, 1H, C$_5$-*β*4), 5.60 (d, J = 3.2, 1H, C$_5$-α2), 4.79 (d, J = 18, 1H, vinyl H$_{trans}$ of *S,S,S*), 3.71 (dd, J = 9 and 3, 1H, vinyl H$_{cis}$ of *S,S,R*), 3.51−3.21 (m, 8H, −CH$_2$CH$_2$− bridge), 2.80 (d, J = 18, 1H, vinyl H$_{trans}$ of *S,S,R*), 2.24 (d, J = 9, 1H, vinyl H$_{cis}$ of *S,S,S*), 1.84−1.14 (m, 8H), 1.29 (br, C*H*$_3$B), 0.70 (s, 3H, Me$_{anti}$ to C$_6$ ring), 0.68 (s, 3H, Me$_{anti}$ to C$_6$ ring), 0.53 (s, 3H, Me$_{syn}$ to C$_6$ ring), 0.27 (s, 3H, Me$_{syn}$ to C$_6$ ring). ^{1}H NMR (C_6D_5Cl, 27 °C, intermediate isomer exchange): δ 7.6−6.8 (br, indenyl and vinyl H$_{int}$ of *S,S,R*; partially obscured by solvent), 6.43 (br, 1H, vinyl H$_{int}$ of *S,S,S*), 6.01 (br, 1H, C$_5$-α1 or α3), 5.80 (br, remaining C$_5$, 7H), 4.86 (br d, 1H, vinyl H$_{trans}$ of *S,S,S*), 3.72 (br, 1H, vinyl H$_{cis}$ of *S,S,R*), 3.6−3.2 (br, 8H, −CH$_2$CH$_2$− bridge), 3.09 (br d, 1H, vinyl H$_{trans}$ of *S,S,R*), 2.36 (br, 1H, vinyl H$_{cis}$ of *S,S,S*), 1.9−1.2 (br, 8H), 1.18 (br, C*H*$_3$B), 0.73 (s, 6H, Me$_{anti}$ to C$_6$ ring), 0.53 (br s, 3H, Me$_{syn}$ to C$_6$ ring), 0.33 (s, 3H, Me$_{syn}$ to C$_6$ ring). ^{1}H NMR (C_6D_5Cl, 91 °C, fast isomer exchange): δ 7.47 (d, J = 7.0, 2H, indenyl), 7.14−6.94 (d, 6H, indenyl, partially obscured by solvent), 6.68 (br m, 1H, vinyl H$_{int}$), 5.89 (d, J = 3.3, 2H, C$_5$-α), 5.84 (d, J = 3.2, 2H, C$_5$-*β*), 4.19 (br s, 1H, vinyl H$_{trans}$), 3.49 (s, 4H, −CH$_2$CH$_2$− bridge), 3.15 (br s, 1H, vinyl H$_{cis}$), 1.74 (br, 1H, CH$_2$), 1.64 (br, 1H, CH$_2$), 1.46 (m, 2H, CH$_2$), 1.04 (br, CH$_3$B), 0.79 (s, 3H), 0.48 (s, 3H). ^{13}C NMR (CD_2Cl_2, −35 °C, both isomers): δ 164.7 (CH=), 162.3 (CH=), 129.4 (CH), 128.1 (CH), 128.1 (CH), 127.9 (CH), 127.9 (CH), 127.8 (CH), 126.2 (CH), 125.2 (CH), 124.5 (CH), 124.4 (CH), 124.0 (CH), 123.7 (CH), 123.4 (CH), 121.9 (CH), 121.6 (CH), 121.1 (CH), 119.0 (CH), 118.5 (CH), 116.8 (CH), 116.4 (CH), 107.4 (CH), 103.7 (CH), 102.7 (CH), 102.1 (CH$_2$=), 99.9 (CH$_2$=), 96.8 (CH), 86.7 (*C*O), 85.6, (*C*O), 48.6 (CH$_2$), 48.6 (CH$_2$), 32.7 (CH$_3$), 31.9 (CH$_2$), 31.6 (CH$_2$), 31.3 (CH$_3$), 30.9 (CH$_2$), 30.8 (CH$_2$), 30.4 (CH$_2$), 29.5 (CH$_3$), 28.4 (CH$_2$), 27.8 (CH$_3$); resonances for the MeB(C$_6$F$_5$)$_3^-$ anion, δ 148.7 (d, J_{C-F} = 237), 137.9 (d, J_{C-F} = 244), 136.8 (d, J_{C-F} = 243), 10.1 (br, MeB); the quarternary carbons of the indenyl ligands and the anion were not observed. ^{19}F NMR (CD_2Cl_2, 15 °C): δ −133.0 (d, J_{F-F} = 21, 2F), −165.0 (t, J_{F-F} = 20, 1F), −166.6 (t, J_{F-F} = 20, 2F). ^{11}B NMR (CD_2Cl_2, 15 °C): δ −13.3. Anal. Calcd for $C_{48}H_{34}BCl_4F_{15}OZr$: C, 49.89; H, 2.96. Found: C, 49.11; H, 3.23.

Generation of [*rac*-(EBI)Zr(OCMe$_2$CH$_2$CH$_2$CH=CH$_2$)][B(C$_6$F$_5$)$_4$] (20b). An NMR tube was charged with *rac*-(EBI)Zr(Me)(OCMe$_2$CH$_2$CH$_2$CH=CH$_2$) (16.0 mg, 0.034 mmol), [Ph$_3$C][B(C$_6$F$_5$)$_4$] (38.8 mg, 0.034 mmol), and C_6D_5Cl (0.5 mL). The tube was maintained at 25 °C and monitored periodically by ^{1}H NMR. [*rac*-(EBI)Zr(OCMe$_2$CH$_2$CH$_2$CH=CH$_2$)][B(C$_6$F$_5$)$_4$] (**20b**) was formed in ca. 60% NMR yield after 24 h. The ^{1}H NMR spectrum of **20b** is identical to that of **20a**, except for the anion resonance.

Generation of [*rac*-(EBI)Zr(OCMe$_2$CH$_2$CH$_2$CH=CH$_2$)(THF)][MeB(C$_6$F$_5$)$_3$] (21). THF (1.5 μL, 0.018 mmol) was added to a solution of [*rac*-(EBI)Zr(OCMe$_2$CH$_2$CH$_2$CH=CH$_2$)][MeB(C$_6$F$_5$)$_3$] (**20a**, ca. 15 mg, 0.015 mmol) in C_6D_5Cl (0.5 mL), and the ^{1}H NMR spectrum was recorded. ^{1}H NMR (C_6D_5Cl): δ 7.47 (d, J = 9, 1H, indenyl), 7.34 (d, J = 9, 1H, indenyl), 7.19 (d, 1H, indenyl), 7.14−6.84 (m, indenyl and solvent), 6.18 (d, J = 3, 1H, C$_5$-indenyl), 5.91 (d, J = 3, 1H, C$_5$-indenyl), 5.88 (d, J = 3, 1H, C$_5$-indenyl), 5.74 (d, J = 3, 1H, C$_5$-indenyl), 5.74 (m, 1H, vinyl H$_{int}$), 5.04 (d, J = 16, 1H, vinyl H$_{trans}$), 5.03 (d, J = 11, 1H, vinyl H$_{cis}$), 3.59 (br s, free THF), 3.54−3.14 (m, 6H, −CH$_2$CH$_2$− bridge and coordinated THF), 3.03 (m, 2H, coordinated THF), 1.74−1.54 (m, free and coordinated THF), 1.44 (m, 2H, CH$_2$), 1.19 (s, 3H, CH$_3$B), 1.06 (m, 2H, CH$_2$), 0.78 (s, 3H, CH$_3$), 0.72 (s, 3H, CH$_3$).

Addition of [NBu$_3$(CH$_2$Ph)][MeB(C$_6$F$_5$)$_3$] to [*rac*-(EBI)Zr(OCMe$_2$CH$_2$CH$_2$CH=CH$_2$)][MeB(C$_6$F$_5$)$_3$] (20a). [NBu$_3$(CH$_2$Ph)][MeB(C$_6$F$_5$)$_3$] (26.0 mg, 0.032 mmol) was added to an NMR tube containing a solution of [*rac*-(EBI)Zr(OCMe$_2$CH$_2$CH$_2$CH=CH$_2$)][MeB(C$_6$F$_5$)$_3$] (14 mg, 0.014 mmol) in C_6D_5Cl (0.6 mL), and the ^{1}H NMR spectrum was recorded at 62 °C. With the exception of the [NBu$_3$(CH$_2$Ph)][MeB(C$_6$F$_5$)$_3$] resonances, the ^{1}H NMR spectrum was identical to that of [*rac*-(EBI)Zr(OCMe$_2$CH$_2$CH$_2$CH=CH$_2$)] [MeB(C$_6$F$_5$)$_3$] (**20a**) without added MeB(C$_6$F$_5$)$_3^-$ salt.

NMR Simulations. NMR spectral simulations were performed using "gNMR" version 3.6.5 (Cherwell Scientific). Simulations of the ZrOC*Me*$_2$ region of **12b** were performed in a two-step procedure. First, the chemical shifts observed for the two Me groups in the slow exchange limit (below −70 °C) were used to set up the spin system, and the relative population ratio was fixed at 1/1 (mole fraction of each site = 0.5). The natural line width in the absence of exchange, W_0 = 1.6 Hz, was measured at −70 °C and confirmed by observation of the same line width at −80 °C. The chemical shifts of the Me resonances (in CD_2Cl_2) vary slightly in the range −100 to −60 °C (δ 1.06−1.11; 1.17−1.22), and a linear extrapolation was used to estimate the chemical shifts at higher temperatures. The observed and calculated chemical shifts for the collapsed resonance at −20 °C (above coalescence) are identical (δ 1.22). Then, for eight temperatures in the range −70 to −20 °C, the exchange rate ($R_{FE,Me}$) was varied to get the best fit between the simulated and the experimental spectra. The first-order rate constant and rate for face exchange are related by $k_{FE,Me} = R_{FE,Me}/0.5$, because the site populations are 0.5. Activation parameters were determined by a standard Eyring analysis (Figure 5). The standard deviations from the least-squares fit were used to estimate the uncertainties in $\Delta H^{\ddagger}$ and $\Delta S^{\ddagger}$.[77]

Simulations of the Me$_{syn}$ region of **20a** were performed using a procedure similar to that described for **12b**. The line width of the Me$_{syn}$ resonances (W_0 = 2.8 Hz) at −16 °C was used as the natural line width in the absence of exchange. The chemical shifts of the Me$_{syn}$ resonances (in C_6D_5Cl) vary linearly with temperature over the range −16 to 21 °C; above the latter temperature coalescence begins. The upfield resonance shifts from δ 0.29 to 0.32, and the downfield resonance shifts from δ 0.53 to 0.54 over this range. The chemical shifts in the absence of exchange at higher temperatures (up to 91 °C) were estimated by linear extrapolation of the −16 to 21 °C values. The observed chemical shift for the collapsed methyl resonance (above coalescence, δ 0.48) agrees within 0.01 ppm with that predicted by averaging the extrapolated chemical shifts of the two methyl resonances. Exchange rates were obtained by comparison of experimental spectra with simulated spectra for 14 temperatures in the range −16 to 91 °C.

Simulations of the H$_\alpha$ and H$_\beta$ region of **20a** were performed for an ensemble of two four-site equal-population exchange systems as described in the text. The chemical shifts observed in the slow exchange limit (below −16 °C) were used to set up the spin systems using a natural line width W_0 = 1.8 Hz and a coupling constant $J_{H\alpha\ -H\beta}$ = 3.2 Hz. The chemical shifts of the H$_\alpha$ and H$_\beta$ resonances (in C_6D_5Cl) vary slightly with temperature between −16 and 20 °C (δ H$_{\alpha1/\alpha3}$ 6.00−6.02; H$_{\alpha2}$ 5.64−5.70; H$_{\alpha3/\alpha1}$ 5.72−5.77; H$_{\alpha4}$ 5.70−5.76; H$_{\beta1/\beta3}$ 5.79−5.81; H$_{\beta2}$ 5.80−5.82; H$_{\beta3/\beta1}$ 5.78−5.80; H$_{\beta4}$ 5.68−5.73). Chemical shifts in the absence of exchange at higher temperatures were estimated by linear extrapolation of the −16 to 20 °C values. Spectra were simulated as described in the text, assuming that the two sets of six possible site-to-site exchanges (α1−α2, α1−α3, α1−α4, α2−α3, α2−α4, α3−α4; *β*1−*β*2, *β*1−*β*3, *β*1−*β*4, *β*2−*β*3, *β*2−*β*4, *β*3−*β*4) all occur at the same rate $R_{\alpha_i\alpha_j}$. Exchange rates were obtained by comparison of experimental spectra with simulated spectra for 14 temperatures in the range 2 to 87 °C. As shown in Figure 8, a good fit was obtained using this procedure. The uncertainty in the exchange rates was probed by extensive simulations using different values for $R_{\alpha1\alpha3} = R_{\alpha2\alpha4}$ and $R_{\alpha1\alpha2} = R_{\alpha1\alpha4} = R_{\alpha2\alpha3} = R_{\alpha3\alpha4}$.

(77) (a) Bevington, P. R. *Data Reduction and Error Analysis for the Physical Sciences*; McGraw-Hill: New York, 1969. (b) Skoog, D. A.; Leary, J. J. *Principles of Instrumental Analysis*, 4th ed.; Saunders College: Fort Worth, TX, 1992; pp 13−14.

Acknowledgment. This work was supported by NSF Grant CHE-9413022 (R.F.J.). J.-F.C. thanks the French "Centre National de la Recherche Scientifique" and Elf Atochem for support. The X-ray structural analyses of **12a** and **20a** were performed by Prof. Jeffery Petersen (West Virginia University) and Dr. Dale Swenson (University of Iowa), respectively.

Supporting Information Available: X-ray diffraction results for **20a**·$CHCl_2CHCl_2$, including tables of crystal data, politional parameters and equivalent isotropic displacement parameters, bond distancces and angles, and anisotropic displacement parameters, and figures showing the molecular structure and atom labeling scheme for the cation and anion and the unit cell diagram (PDF). This material is available free of charge via the Internet at http://pubs.acs.org.

JA000989P